2007 Wilhelm Award Article

Toward an Enhanced Understanding and Implementation of Photopolymerization Reactions

Christopher N. Bowman and Christopher J. Kloxin
Dept. of Chemical and Biological Engineering, University of Colorado, Boulder, CO 80309

DOI 10.1002/aic.11678
Published online October 6, 2008 in Wiley InterScience (www.interscience.wiley.com).

Photopolymerization reactions proceed rapidly at ambient conditions and are able to exhibit both temporal and spatial control, nevertheless their full potential has been limited by a lack of understanding of the polymerization kinetics and polymer network evolution as well as a lack of custom, functional monomers, and polymerization mechanisms. For the last 15 years, our group has sought to address these limitations by reaction engineering at both the fundamental and applied levels with a focus on increasing the understanding, potential, and implementation of photopolymerization reactions. In particular, we have modeled and experimentally validated the complex spatially dependent polymerization kinetics and network heterogeneity, and we have implemented these systems for applications improvement or development in lithography, microdevice fabrication, biomaterials, biodetection, dental materials, and surface coatings. © 2008 American Institute of Chemical Engineers *AIChE J,* 54: 2775–2795, 2008

Keywords: photopolymerization, reaction kinetics, kinetic modeling, thiol-ene, iniferter

Introduction

Since their use by the ancient Egyptians as an integral part of the mummification process,[1] photopolymerization reactions have continued to be ubiquitous reactions with significant capabilities that more traditional polymerizations do not possess. These characteristics, including the ability to cure rapidly at ambient conditions[2,3] and with intimate control in both time and space when and where the polymerization occurs,[4–6] have enabled photopolymerizations to be implemented in a wide range of applications that are as diverse as dental materials,[2,7–10] contact and other lenses,[11–13] coatings,[14–17] photolithography,[4,18–20] microfluidic device fabrication,[4,5,21–24] tissue engineering matrices,[25–27] and 3D prototyping.[28,29] Unfortunately, despite the vast potential for energy efficient, solvent-free reactions that are able to be performed rapidly at ambient conditions, the range of applications where photopolymerizations are utilized is limited by a general lack of understanding of the polymerization process itself as well as a lack of solutions for persistent problems associated with volume shrinkage and stress,[9,30–33] oxygen inhibition,[1,34–38] and the presence of unreacted, potentially extractable monomer.[34,39–41] For the last 15 years, our group has sought to develop enhanced understanding, including both experimental and modeling approaches, of these reactions while simultaneously utilizing that understanding to address the problems that limit the implementation of photopolymerizations.

At its core, the traditional radical-mediated photopolymerization reaction is quite simple, consisting of photoinitiation, propagation, termination, and chain transfer reactions as illustrated in Figure 1; however, in nearly all practical photopolymerization systems, the polymer formation is simultaneously associated with dramatic material property changes. Although these materials are initially low viscosity liquids, they are rapidly, frequently in less than a second, converted into glassy, highly crosslinked materials. This dramatic evo-

Correspondence concerning this article should be addressed to C. N. Bowman at Christopher.bowman@colorado.edu.

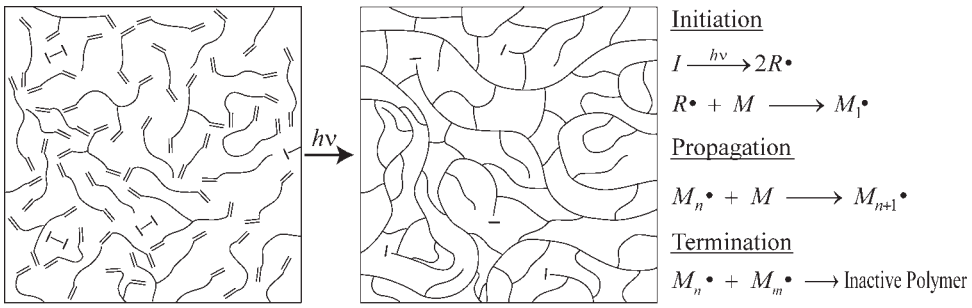

Figure 1. Illustration of the photopolymerization reaction process and the chemical reaction steps involved in the photopolymerization.

Typical photopolymerization reactions occur on the order of seconds and involve multiple distinct monomers. The final polymer product is nearly always crosslinked and frequently exhibits a glass transition temperature far above ambient or curing conditions. The crosslinking reaction necessitates reaction engineering of the polymerization system as the polymer product resulting from the reaction is inalterable in shape and polymer structure by postreaction treatments such as heating or extrusion.

lution of the material properties has significant consequences for the polymer behavior, leading to complexities in the reaction system that include diffusion controlled reactions,[34,42–49] delays in the attainment of equilibrium properties,[34,39,50] concentration, light intensity, and temperature gradients,[51,52] and pronounced heterogeneities in the crosslink density.[53–57] Each of these tendencies makes the polymerization reaction and the polymer properties highly dependent on the conditions under which the material is polymerized, making it critical to understand and manipulate the formation-structure-property relationships that exist for these reactions and materials.

The importance of these relationships in photopolymerization reactions is further heightened by the inability to manipulate the polymer properties, shape, or structure postpolymerization. Because these reactions nearly always involve the formation of a crosslinked structure, very little postpolymerization manipulation of the polymer is feasible. For linear polymers, the primary molecular structure and molecular weight distribution of the polymer are fixed during the polymerization reaction, but subsequent processing, such as melting, extrusion, annealing, etc., can readily modify the polymer properties and shape. For *in situ* formed crosslinked polymers, such manipulation and alteration of the material characteristics is not possible, highlighting the need for polymerization reaction engineering, molecular design of monomers, and the development of improved polymerization mechanisms.

Figure 1 presents the photopolymerization mechanism for a classical, radical-mediated polymerization. This mechanism involves the generation of radicals by one of a variety of methods. Both type I (direct cleavage) and type II (sensitization) initiators have readily been used to initiate free-radical polymerizations with type I reactions more commonly used for UV initiation and type II initiators more commonly used for visible light initiation.[1,58,59] The initiation reactions are those in which the initiator, I, decays into primary radicals, $R\bullet$, which subsequently react with unreacted carbon–carbon double bonds to initiate polymer formation; the typical assumption is that the initiator forms two relatively equally reactive primary radicals which then react to initiate polymerization. The initiation reaction is the only one involving direct interaction of the material with light; however, for strongly absorbing initiators, thick polymerizing systems, or dyed or pigmented films, a significant gradient in light intensity, and therefore initiation rate, is established within the polymerizing film.[60] At a given location within the film the initiation rate, R_i, is described by

$$R_i = 2f\phi\varepsilon[I]I_0, \tag{1}$$

where both the light intensity, I_0, and initiator concentration $[I]$ may depend on the position within the film, and ε, f, and ϕ are the initiator molar absorptivity, efficiency, and quantum yield, respectively. One significant complication is that many of these factors change throughout the polymerization, particularly as the extent of reaction increases and mass transfer becomes more difficult. In particular, it is well recognized that the initiator efficiency changes throughout the reaction with primary radicals less readily escaping the solvent cage and tending to recombine into nonreactive products.[1,34,51,61] Despite this effect, the initiation reaction is generally the most ideal and least affected by mass and heat transfer limitations of the various reactions occurring during the crosslinking photopolymerization.

The propagation reaction generally involves radical species growth by the radical addition to a carbon–carbon double bond, generating a new radical at the end of the polymer chain as shown in Figure 1. This bimolecular reaction between the radical and the double bond is generally assumed to be chain-length independent[62] though there are clearly indications that the oligomer/polymer chain length does have a significant effect for degrees of polymerization below 10–50, depending on the polymer being formed.[49,62,63] Further, as the crosslinking density increases throughout the reaction, leading to the eventual vitrification of the polymer, this bimolecular reaction rate is reduced because of diffusional limitations. Overall, the propagation reaction rate is generally written as

$$R_p = k_p[M][M_n\bullet], \tag{2}$$

where k_p represents the propagation rate constant, $[M]$ represents the double bond concentration, and $[M_n\bullet]$ represents the

total propagating radical concentration. The propagation reaction encompasses numerous reactions including the reactions of both pendant and monomeric double bonds,[34,64–66] the reinitiation of radicals formed by chain transfer, and reactions of the various radicals that exist at any point during the polymerization, including those in dramatically different environments.[34,67–69] This idealization effectively renders the propagation kinetic constant a lumped parameter that is suitable for describing these various reactions as they relate to the overall polymerization kinetics.

Generally, the termination reaction is presumed to be a bimolecular reaction involving two radicals, as shown in Figure 1. The kinetics of this reaction are ideally written assuming no chain length dependence, no effects of the polymer heterogeneity, and no radical trapping as

$$R_t = 2k_t[M_{n\bullet}]^2, \tag{3}$$

where k_t is the termination rate constant. Here, diffusional limitations are more pronounced than on any other polymerization step. Classically, autoacceleration (also referred to as the gel effect or the Trommsdorff effect) has played a significant role in many bulk polymerizing systems.[43,44,49,63,70] This phenomena occurs when the termination reaction becomes diffusion controlled. Then, as mass transfer becomes ever more difficult, the radical concentration increases, sometimes by many orders of magnitude,[34,67–69] leading to a significant polymerization rate increase despite the decreasing double bond concentration.

Highly crosslinked polymers, frequently formed during photopolymerizations, often present an additional complexity in the termination, where many radicals cease to propagate, becoming "trapped" in the highly crosslinked polymer regions. These radicals are isolated from unreacted double bonds and effectively terminated, at least in regards to their ability to polymerize on reasonable timescales, but they remain present in the polymer for months or years.[34,67–69] Although the radical concentration is measurable by electron spin resonance spectroscopy during and after the polymerization, such measurements are relatively impractical for most photopolymerizations, thus a pseudo steady-state assumption is applied for the radical concentration to express the polymerization rate as,

$$R_p = k_p[M](R_i/2k_t)^{1/2}. \tag{4}$$

A variety of other reactions are also occurring during these polymerizations that significantly complicate their behavior. Inhibition by oxygen is one of the most prevalent and pervasive limitations on free-radical photopolymerizations. Oxygen very rapidly reacts with the propagating radical to form a peroxy-based radical. This peroxy radical is quite unreactive towards propagation, though it is readily able to abstract hydrogens from species such as amines and thiols. The lack of propagation reactivity effectively enables oxygen at typical concentrations of dissolved oxygen in monomers to inhibit the polymerization completely.[1,35–38] In thicker films, where oxygen diffusion is unable to replenish that consumed by the peroxy formation, the polymerization eventually proceeds in deeper regions of the film. Additionally, chain transfer reactions to the polymer backbone are known to be a significant complication in many reactions, particularly those involving acrylate polymers.[59,71–73]

In addition to the kinetic complexities that arise during these reactions, spatial variations in the crosslink density and other species distribution are also prevalent. These heterogeneities lead to polymer networks that have glass transition temperature regions that are more than 150°C in breadth[34,55,74,75] and in which relaxation times vary by as many as 18 orders of magnitude within the same polymer network.[56] In the earliest stages of the reaction, radicals are formed from initiator cleavage with initiation sites well dispersed within a nearly infinite pool of unreacted monomer, which yields a locally high degree of polymerization, promoting intramolecular crosslinking (or primary cyclization) of these radicals and leading to microgel formation.[34,76,77] The relatively high conversion of pendant functional groups in microgels ultimately does not lead to significant network development. These "wasted" crosslinks delay the gel-point significantly, often by as much as 5–10% conversion, from the classical predictions, many of which would predict ideal gel-points in these systems to be below 1% double bond conversion. At the later stages of the polymerization, following macroscopic gelation and approaching vitrification, the nature of the heterogeneity inverts and unreacted nanoscale pools of monomer form throughout the otherwise highly crosslinked polymer network. These pools, which frequently do not contain unreacted initiators, are not able to polymerize, and the unreacted monomer remains for the useful lifetime of the polymer film. The complex nature of this heterogeneity has previously not been well quantified or described despite its significant effect on the material properties.

Despite these numerous complexities, radical-mediated photopolymerizations remain one of the most facile and capable polymerizations. They are capable of rapidly polymerizing monomer formulations, in a spatially and temporally controlled manner, into highly crosslinked, functional polymeric materials. To take advantage of these capabilities, however, it is clear that several aspects of photopolymerization require both development and understanding. Our research over the last 15 years has focused on doing exactly that and enhancing the basic understanding of the formation-structure-property relationships as well as developing novel polymerization methodologies and newly synthesized, more functional monomers that both improve existing applications and facilitate the entry of photopolymerizations into applications for which it was previously unutilized. The remainder of this manuscript addresses fundamental developments in the reaction engineering and polymerization kinetics of photopolymerization reactions, the development of novel polymerization methodologies, and the implementation of these systems.

Polymerization Kinetics

An illustration of typical photopolymerization kinetic behavior is presented in Figure 2a, where the polymerization rate is plotted as a function of the double bond conversion for two different photoinitiation rates. Two polymerization regimes are clearly identifiable in each curve and are typical

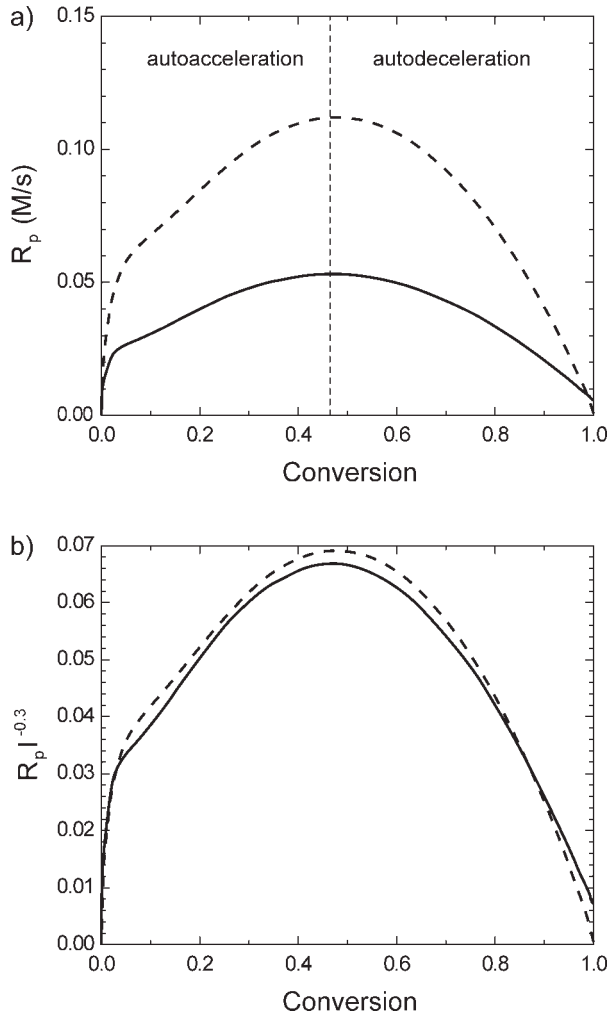

Figure 2. (a) Polymerization rate and (b) polymerization rate normalized by the initiation rate to the exponent of 0.3 vs. conversion for PEG600DMA at irradiation intensities of 5.0 (dashed line) and 0.5 (solid line) mW/cm^2.

Figure adapted from ref. 48.

of the kinetics observed during crosslinking photopolymerization reactions. These regimes have classically been referred to as the autoacceleration regime, where the polymerization rate increases despite the monomer consumption, and the autodeceleration regime, where the polymerization reaction slows down and ultimately stops despite the continuing presence of both the radical and monomer reactants.[2,7,34] Both behaviors are dictated by the mobility changes of radicals and unreacted double bonds as a result of the continuing polymerization and crosslinking.

At the end of the polymerization, autodeceleration results from the vitrification of the polymerizing mixture. At this stage, the propagation reaction becomes diffusion controlled as the rate at which double bonds are able to diffuse to the radicals becomes rate limiting. Each subsequent reaction further reduces the species motilities, ultimately ceasing the polymerization reaction despite continued initiation and a radical concentration that can be as high as 10^{-3} M.[34,68,69]

During autoacceleration the termination reaction, a biomolecular reaction between two radicals, becomes diffusion controlled and the reduction in mobility, as a result of the continuing polymerization and crosslinking, further reduces the termination kinetic constant. The reduction in the termination kinetic constant results from more hindered termination and leads to an increase of potentially several orders of magnitude in the radical concentration, driving the observed rate increase. Uniquely, in crosslinked systems the radical mobility as a result of classical diffusion mechanisms drops to such an extent that the radicals actually become more mobile by propagating than by diffusion. This unique mobility mechanism for radicals is referred to as reaction diffusion controlled termination[42–44,46,47,49,63,70] and has been observed throughout a large portion of crosslinking polymerizations as well as at high monomer conversions in linear systems. Ultimately, reaction diffusion controlled termination leads to a proportionality between the propagation frequency and the termination kinetic constant,[44–46,78,79]

$$k_t = R\,k_p[M], \tag{5}$$

where R represents the reaction diffusion constant.

In addition to being complicated by reaction diffusion and changing mobility throughout the reaction, the termination reaction was determined to be highly dependent on the initiation rate as it effects the kinetic chain length. An example of this result is illustrated experimentally in Figure 2b where the polymerization rate is scaled by the initiation rate raised to the exponent of 0.3. Here, the polymerization rate does not scale with the classical, idealized 0.5 exponent because, as the initiation rate increases, the kinetic chains become shorter and the radicals more mobile so that they terminate more rapidly. Ultimately, this complex behavior results in a termination kinetic constant that must account for radicals of length i terminating with radicals of length j,[80–82]

$$k_t^{i,j} = k_{t_0}^{1,1}\left\{1+\left[\frac{Rk_p[M]}{k_{t_0}^{1,1}}+\frac{1}{2}\left(\frac{1}{i^{\alpha}}+\frac{1}{j^{\alpha}}\right)e^{-A_f\left(\frac{1}{f}-\frac{1}{f_{ct}}\right)}\right]^{-1}\right\}^{-1}, \tag{6}$$

where α represents an exponent that describes the relationship between mobility and termination, $k_{t_0}^{1,1}$ represents the termination kinetic constant between two radicals of length one, f is the fractional free volume, and f_{ct} is the critical free volume at which termination transitions to diffusion control. Equation 6 is used to predict the conversion and chain length dependent termination constant as shown in Figure 3. Here, the various regions of the polymerization are obvious as initially, during autoacceleration, there is a significant dependence of the termination constant on chain length as well as conversion with higher chain lengths and higher conversions giving rise to lower termination constants, as observed experimentally.[73] As the conversion increases to 25–40%, reaction diffusion becomes dominant, and the decrease in the conversion dependent termination constant is mitigated until after 40% conversion, where the propagation reaction becomes diffusion limited and autodeceleration takes over.

Once the kinetic constants for propagation and termination were modeled, it was possible to incorporate mass transfer

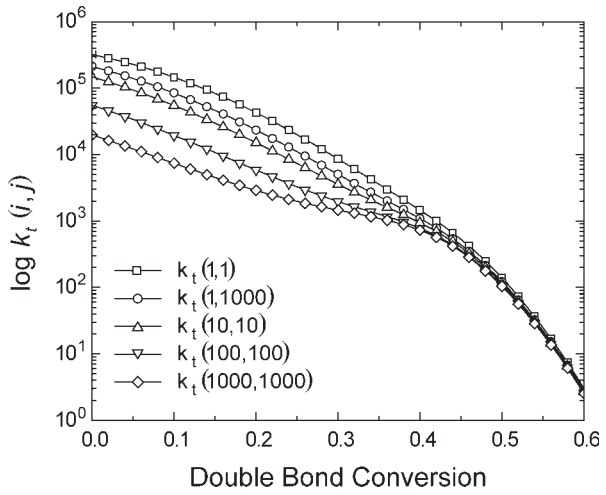

Figure 3. Model predictions of the chain length dependent termination kinetic constant as a function of chain lengths and double bond conversion, where *i* and *j* are the chain lengths of the two terminating radical species.

Here, the chain length dependence is most prominent at the early stages of the reaction, during autoacceleration and is largely absent at the higher conversions where reaction diffusion controlled termination dominates the termination reaction process. Figure adapted from ref. 80.

and heat transfer rates as well as the temperature dependence of the reaction rates. Through several generations of model development, we have been able to arrive at a successful model which is suitable for predicting spatially dependent polymerizations of the type generally used industrially for a broad range of applications.[37,52,83,84] Figure 4 presents just such a prediction for a photopolymerized film. Here, it is obvious that diffusion of oxygen back into the sample from the air-sample interface continues to inhibit the polymerization and leads to the commonly observed tacky or unpolymerized film on the sample top. Throughout the remainder of the polymerizing film, high conversions are achieved; however, the bottom of the film reaches the highest conversion because the bottom surface of the sample is insulating and the maximum temperature occurs at the bottom interface.

In addition to modeling the spatial dependence of the polymerization, determination and understanding of the complex formation-structure-property relationships in photopolymerizations of multiple monomers through high throughput techniques[6,85–88] and modeling facilitates true materials design. In this work, we were able to determine via high throughput methodologies polymerization kinetic and polymer property parameters for more than ten distinct monomers. These models were then used to ascertain an optimal monomer formulation that combined any amount of each of the monomers while being optimized with respect to minimum cost and achieving all necessary polymer and polymerization properties. Figure 5 illustrates the predictions for the kinetics and various material properties that are achieved after 30 s of polymerization for all possible ternary compositions of three monomers, including one monoacrylate and two diacrylates. This data illustrates the results achieved for only one ternary combination of the monomers where all possible ternary or higher combinations can be evaluated and considered in the optimization.

Throughout our experimental and modeling studies, it has become apparent that physical constraints on polymerization are critical in determining the overall polymerization rates and the ultimate material properties.[89–92] This behavior was found to be particularly critical in systems where the polymerization is essentially performed in a nanoreactor, where the "reactor" is, in fact, a templated, self-assembled molecular environment. One such environment that was thoroughly studied was the polymerization of small amounts of monomer within a liquid crystal.[89,91] As illustrated in Figure 6, we demonstrated that polymerizations in ultrathin monomer films of a few nanometers in thickness as controlled by the smectic layering of the liquid crystal lead to dramatically inhibited termination reactions and higher radical concentrations than would be achieved otherwise, ultimately accelerating the polymerization rate by as much as a factor of three. Identical polymerizations performed in an isotropic host were significantly slower with lower radical concentrations, despite being performed at elevated temperatures.

In addition to analyzing, predicting, and understanding classical polymerizations of commercially available monomers, our laboratory has focused on engineering polymerization reactions by synthesizing novel monomers[3,93–97] as well as developing or implementing distinct photopolymerization mechanisms that enable capabilities that are not possible with classical systems.[98–101] In one particular example, we have focused on synthesizing monomers that exhibit extremely fast photopolymerization reactions[3,27,93,97,102] despite being monovinyl in character, which are typically at least an order of magnitude slower than multifunctional (meth)acrylate monomers. Subsequently, we have focused extensively on understanding the structure-property relationships that give rise to the unique reactivity associated with these ultrarapidly polymerizing monomers. The importance of molecular structure to monomer reactivity is illustrated in Figure 7. Systematic variations in the molecular structure, far removed from the reactive acrylic double bond, have dramatic effects on the reactivity as shown in Figure 7a, where a single atom has been changed from a nitrogen to a oxygen to a carbon (i.e., from an ester to a carbonate to a carbamate moiety). These effects are a combination of electronic effects including changes to the propagating active center, hydrogen bonding, and molecular dipole.[1,103–105] Understanding the impact of various substitutions on monomer reactivity allows for the design of monomethacrylate monomers that are at least as reactive as diacrylate monomers. This result is illustrated in Figure 7b where the reactivity of a benzyl carbamate methacrylate (BCMA) is compared with the reactivity of several classical photopolymerizable monomers including a diacrylate, a dimethacrylate, and a traditional monomethacrylate, all at the identical initiation conditions. The BCMA is orders of magnitude more reactive than any of the methacrylates, reaching a higher maximum conversion and having comparable reactivity to the multifunctional acrylate.

The development of these novel, highly reactive materials has, in particular, facilitated the implementation of these materials in biomedical applications that demand high

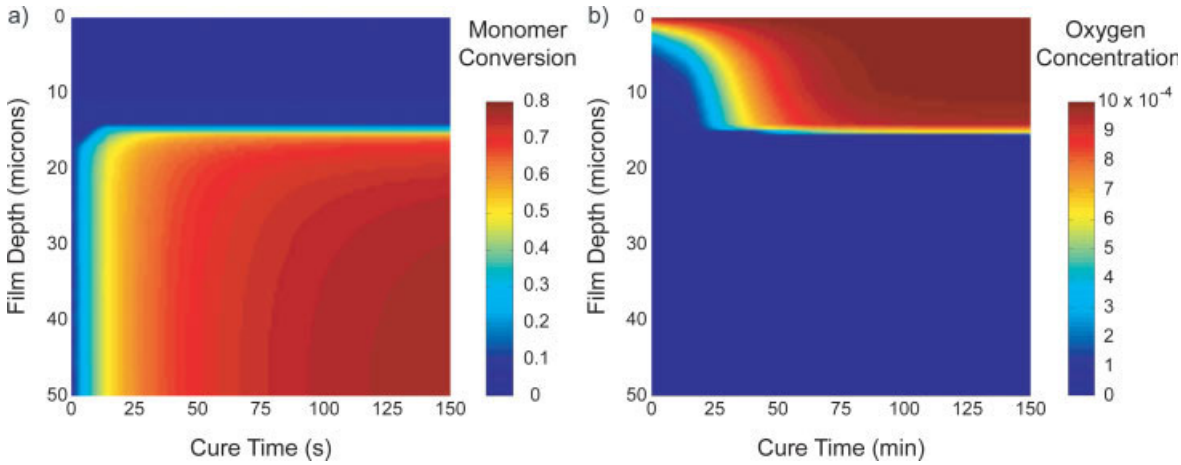

Figure 4. Theoretical predictions of the double bond conversion and oxygen concentration as a function of film depth and time.

Here, the film is assumed to be open at the top to atmospheric oxygen with a convective heat transfer boundary condition at the top and an insulating boundary at the bottom for both heat and mass transfer. An unpolymerized layer forms on the sample top due to oxygen transport back into the sample during the curing process. Figure adapted from ref. 37.

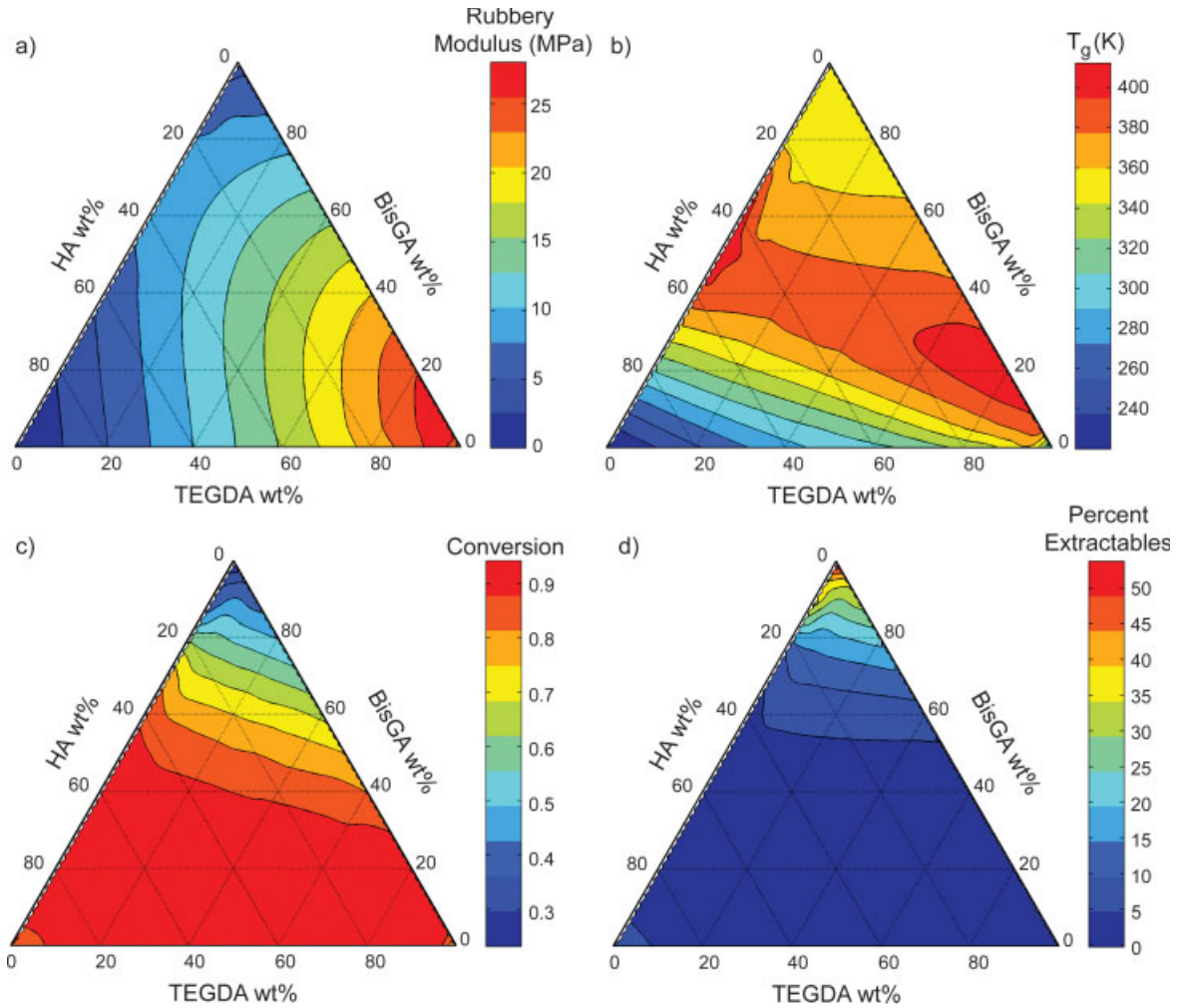

Figure 5. Theoretical predictions of the (a) rubbery modulus, (b) polymer glass transition temperature, (c) double bond conversion, and (d) percent extractable monomer for all possible ternary compositions of hexyl acrylate (HA), triethelyene glycol diacrylate (TEGDA) and bisphenol A diacrylate (BisGA) monomers.

These predictions are all for 30 s of exposure time at 3.5 mW/cm^2 with 0.5 wt % dimethoxyacetophenone used as an initiator.

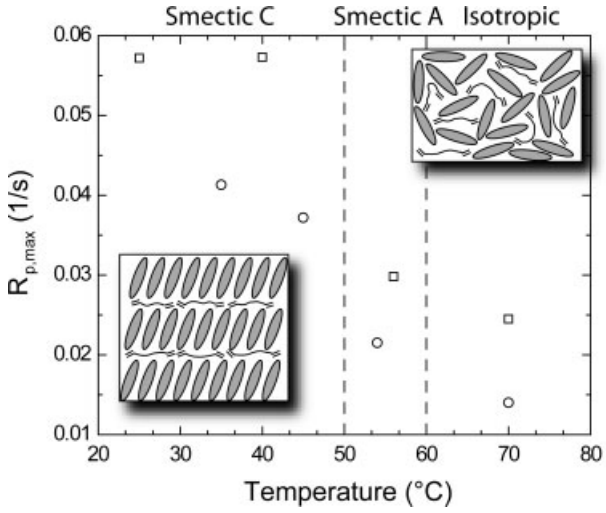

Figure 6. Polymerization rate as a function of temperature and self-assembled structure of monomer-liquid crystal composite systems.

Liquid crystal phases are at the top of the graph with dashed lines for the phase transition temperatures. These systems organize the monomer in a nanoreactor associated with self-assembly of the liquid crystalline environment at low temperatures and exist as isotropic solutions at higher temperatures. In contrast to traditional polymerization behavior, the rate accelerates in the lower temperature, more organized state. Polymerization rates are for the photopolymerization of hexanediol diacrylate in a ferroelectric liquid crystal mixture of 1:1 W7 and W82. Figure adapted from ref. 91.

degrees of conversion and rapid curing.[2,7,95,106,107] For biomedical materials, the risk of leachable unreacted monomer is significant and has lead to the utilization of dimethacrylates as typical photopolymerizable reactive diluents because, once either one of the methacrylate groups reacts, the monomer is no longer extractable. Furthermore, dimethacrylate reactive diluents polymerize far more rapidly than conventional monomethacrylates. In the dental materials field, however, we have recently shown that the inclusion of one particular novel monomer, morpholine carbonyl methacrylate as a 30% reactive diluent in bisphenol A dimethacrylate, increases the polymerization rate by a factor of more than three while also increasing the conversion and modulus of the composite dental filling.[95,107] Thus, this monomer overcomes all of the disadvantages of the monomethacrylates by reacting more rapidly and to a much greater conversion.

Thiol-Ene Photopolymerization Reactions

Unfortunately, despite the broad applicability of photopolymerizations and their outstanding characteristics, the traditional (meth)acrylate-based free radical photopolymerization process is limited by an array of drawbacks that include oxygen inhibition, the presence of residual, unreacted monomer, slow curing, and polymerization induced shrinkage and shrinkage stress development.[2,7,10,34] These limitations to traditional photopolymerization are all potentially solved by the utilization of thiol-ene-type photopolymerization reactions.

The thiol-ene photopolymerization represents a fundamental shift in the mechanism of photopolymerizations in which the reaction proceeds via alternating propagation and chain transfer reactions (see Figure 8). This behavior leads to a step-growth evolution of a network that is photoinitiated and radically-mediated, having significant advantages related to delayed gelation such as limited extractables and reduced shrinkage and shrinkage stress.[59,108–110] Furthermore, peroxy radicals, formed by radical attack on oxygen and typically

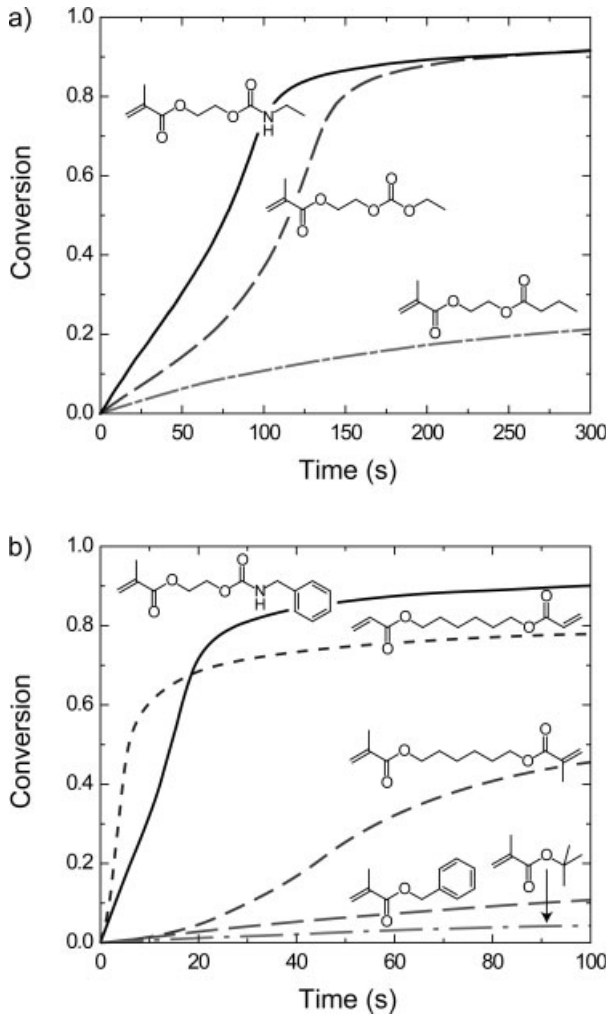

Figure 7. Double bond conversion as a function of time demonstrating the importance of molecular structure on monomer reactivity.

Here, in (a) systematic variations at a single atomic position are shown to have a pronounced effect on the polymerization kinetics, despite being far from the polymerizable double bond. In (b) a comparison is made between a highly reactive monomethacrylate monomer and classical photopolymerizable systems including a diacrylate, a dimethacrylate, and a traditional monomethacrylate. Here, structural modifications to the BCMA monomethacrylate enable the polymerization to proceed more than 100 times faster than the traditional monomethacrylate. Figure adapted from ref. 3.

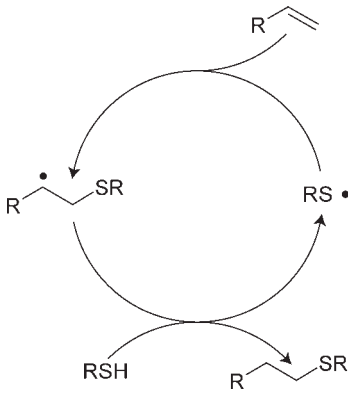

Figure 8. Illustration of the ideal thiol-ene polymerization mechanism in which the propagation and chain transfer reactions continually cycle, proceeding at equal rates without any significant homopolymerization of the ene group.

This mechanism leads to a simple coupling reaction that results in the addition of the thiol across the ene functional group, causing the molecular weight evolution to occur via a step-growth mechanism.

unable to propagate, can abstract a hydrogen from a thiol group, forming a thiyl radical, and thus thiol-ene polymerizations are resistant to oxygen inhibition. Unfortunately, the thiol-ene photopolymerization itself has been limited by a lack of exploration and a lack of appropriate, available materials. Our work in this area has focused on advanced experimental characterization and modeling of the reaction[87,101,111–116] and network evolution[117–120] as well as the implementation of improved thiol-ene polymerizations in liquid crystals,[92] polymer-derived ceramics,[121,122] dental materials,[8,123] high glass transition temperature, low stress materials,[8,124] hydrogels,[26,125,126] photolithography,[20,127,128] and surface modification reactions.[15,16,20,127,129]

One of the unique aspects of the thiol-ene photopolymerization process is that it is able to be photoinitiated even in the absence of a distinct initiator species.[59,100] The absence of an initiator enables several distinct advantages of the polymerization over those that include initiator including the ability to cure very thick films, limiting the volatile and colored by-products typically associated with initiator decomposition, eliminating residual initiator light absorption, improving film clarity, and enhancing the stability of the polymer film. Figure 9 presents the photoinitiatorless polymerizations of a single thiol-ene formulation at two different irradiation conditions representing low intensity, low wavelength irradiation and high intensity, high wavelength irradiation. Both polymerizations proceed rapidly despite the lack of an initiator, but the lower wavelength polymerization proceeds more rapidly despite being initiated at 100 times lower light intensity. It was determined that the mechanism of the self-initiation reaction at the lower wavelengths involves the direct absorption of a photon by the thiol followed by cleavage of the thiol into a thiyl and hydrogen radical, each of which, through one or a series of reactions, is likely to initiate polymerization.[113] The initiation mechanism at the higher wavelength is yet to be determined, but found to be first order in the concentration of the "ene" monomer for all the systems studied.[113] The difficulty in assessing this initiation mechanism results from the extremely low molar absorptivities of all the compounds that participate in the thiol-ene reaction at these longer wavelengths.

The step-growth nature of the thiol-ene reaction affords numerous advantages for this reaction including the increased gel-point conversion,[120,130] reduced shrinkage per vinyl group that polymerizes,[8,123] and significantly enhanced control of the polymer molecular weight, homogeneity, and network structure when compared with chain-growth radical reactions. In particular, we have demonstrated that thiol-ene grafting reactions afford many of the same advantages of controlled radical polymerizations (relatively low polydispersity, uniform grafting, and ability to graft thin films) while also possessing the high reactivity and photopatternability of a photopolymerization reaction. In Figure 10, we present a demonstration of the ability to control the polymer graft molecular weight and graft thickness on the 10–20 nm scale. Here, crosslinked thiol-ene polymer features with size scales on the order of hundreds of nanometers are formed by step and flash lithography[20,131] of a thiol-ene mixture that contained a small amount of excess thiol. The residual thiol that exists following the reaction facilitates grafting of a linear thiol-ene polymer that is appropriate for reducing the feature size in a controlled manner. The linear polymer grafting formulation is intentionally stoichiometrically imbalanced to control the polymer molecular weight by the step-growth reaction mech-

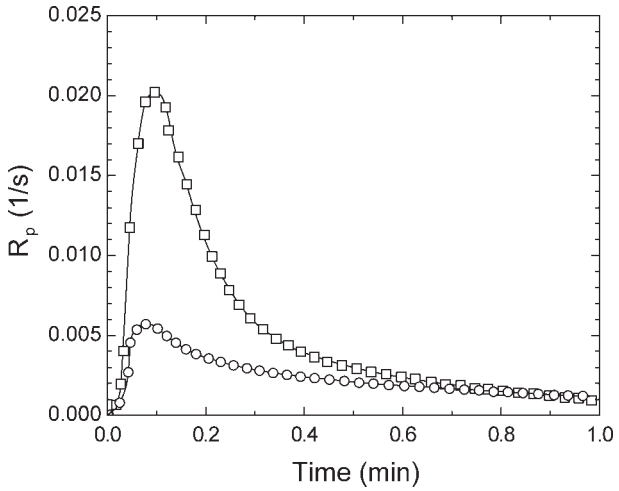

Figure 9. Initiatorless photopolymerizations of thiol-ene reactions initiated by varying wavelengths of light.

Here, the polymerization rate of a stoichiometric mixture of triethylene glycol divinyl ether and pentaerythritol tetrakis(3-mercaptopropionate) is plotted as a function of time for two distinct irradiation conditions: 254 nm at 0.8 mW/cm^2 (□) and 365 nm at 80 mW/cm^2 (○). These results indicate that both polymerizations proceed on reasonable timescales and to high conversions despite the absence of an initiator species. The self-initiation reaction and subsequent polymerization are much more rapid with the lower 254 nm irradiation than the 365 nm irradiation, despite the higher intensity at the longer wavelength. Figure adapted from ref. 100.

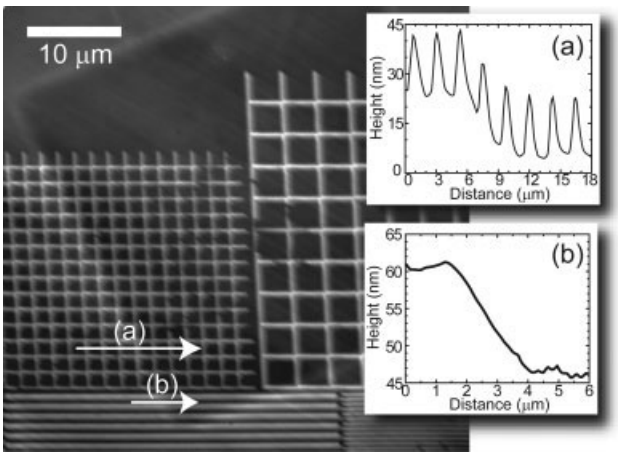

Figure 10. Atomic force micrograph of secondary micropatterned polymer layer containing a triethylene glycol divinylether-pentaerythritol tetrakis(3-mercaptopropionate) (thiol-:ene = 0.35:1) with 0.01% DMPA polymerized on nanopatterned replica by exposing to UV light (365 nm, 15 mW/cm^2 for 3 min) through a photomask with 50 μm square, and the insets show the height profiles along lines (a) and (b).

Figure adapted from ref. 20.

anism. The manipulation of the molecular weight in this self-limiting manner enables the feature sizes to be controlled systematically simply by changes in the thiol-to-ene ratio. The Figure 10 insets demonstrate the ability to photolithographically pattern the grafting reaction such that feature sizes are appropriately changed only where the light is incident, enabling a powerful combination of controlled, spatially modulated feature size reduction.

Despite the advantages associated with thiol-ene polymerization reactions, their step-growth nature significantly limits the crosslinking density and glass transition temperature that are achieved from these ideal, step-growth reactions. As such, we have found a dramatic benefit in evaluating multicomponent thiol-ene-vinyl polymerizations where the polymerization mode is mixed between step-growth, involving alternation of propagation and chain transfer (with the ene) and chain-growth associated with homopolymerization/self-propagation reactions of the vinyl groups. These thiol-ene-acrylate[120,132] and thiol-ene-methacrylate[133,134] polymerizations have several distinct benefits associated with a semi-ideal combination of the two polymerization modes in a single polymerization. In the case of the thiol-ene-methacrylate polymerization, the polymerization frequently proceeds largely through the methacrylate homopolymerization at early stages of the reaction followed by a more step-like thiol-ene polymerization at the end.[133,134] Liquid-gel phase separation facilitates the *in situ* formation of a composite material. The thiol-ene-acrylate polymerization is more uniform throughout the reaction, enabling high conversions and crosslink densities to be achieved in the polymers formed. The kinetic and structural modeling of these ternary polymerization reactions must include an array of complex reactions as summarized in Figure 11. Figure 12 shows the experimental results and predictions of the kinetic model for the conversion of each component in the ternary polymerization reaction. These predictions are in excellent agreement with the experimental results suggesting that mass transfer limitations on propagation and termination are not significant. It is worth noting that the mechanical properties and particularly the glass transition temperature of the ternary thiol-ene-acrylate systems are frequently nearly equivalent to those of the pure acrylate while forming a more homogeneous network with lower residual stress.[132]

Structural Heterogeneity in Highly Crosslinked Polymer Networks

The basic photopolymerization mechanism for the formation of highly crosslinked networks leads both to high internal stress associated with the polymerization shrinkage and to heterogeneous networks with regions of both high and low crosslink density. This heterogeneity leads to stress gradients within the network, brittleness, and the presence of a higher than expected level of completely unreacted monomer.[34] The approach to combat these deleterious effects has been first to understand the complex relationships between the molecular structure of the monomers, the polymerization mechanism and kinetics, mass transfer of the various species present in the reaction, and the reaction conditions imposed on the photopolymerization. Mitigation of the heterogeneity and the resulting stress has been achieved both by changes to the polymerization mechanism, including the introduction of controllably reversible covalent bonds into the network[135,136]

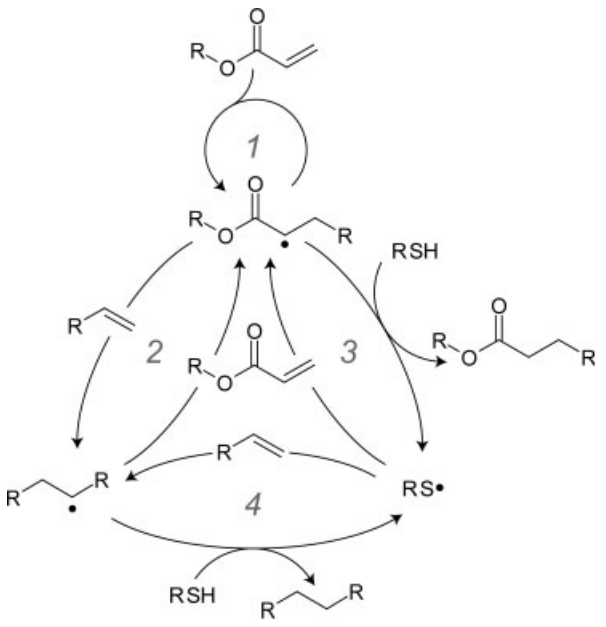

Figure 11. Thiol-ene-acrylate reaction mechanisms, composed of 4 cycles: (1) Homopolymerization of the acrylate, (2) copolymerization of the ene and acylate, and the (3) thiol-acrylate and (4) thiol-ene polymerization.

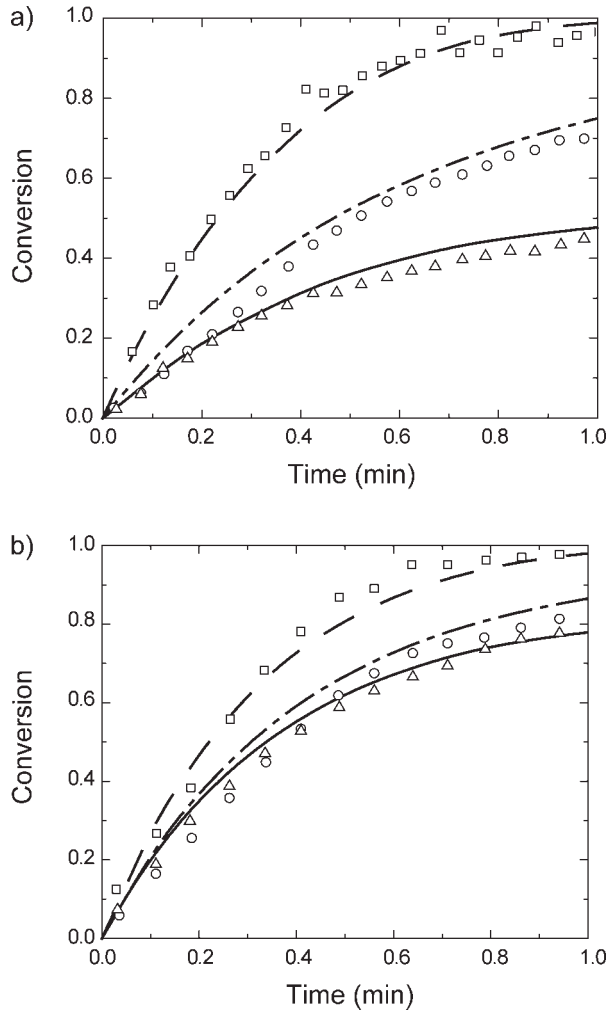

Figure 12. Model predictions (lines) and experimental data (symbols) for conversion versus time of ternary thiol-vinyl ether-acrylate photopolymerizations.

Thiol (□, dashed line), vinyl ether (△, solid line), and acrylate (○, dash-dotted line) conversions were performed for initially (a) 0.5:1:1, and (b) 2:1:1stoichiometric ratios of thiol-vinyl ether-acrylate functionalities. The samples were formulated with 0.1 wt % dimethyl phenyl acetophenone and irradiated at 365nm, 2 mW/cm^2. Figure adapted from ref. 115.

as well as the utilization of the step-growth thiol-ene reactions described above.[8,123]

The mechanistic origins of heterogeneity are best illustrated by considering the classical picture of a free-radical vinyl polymerization, where the initiation reaction triggers a cascade of reactions between the growing radical and a large number of monomers. Each reaction adds another monomer unit to the end of the polymer chain, converting double bonds into single bonds, and transferring the propagating radical to the next monomer. This reaction cascade occurs within a local region roughly defined by the location of the initial radical formation and the size of the macroradical being formed. For highly crosslinked networks, where monomers are multifunctional, the polymeric tail led by the propagating macroradical contains a significant number of pendant vinyl groups. These pendant vinyl groups, because of their proximity to the growing polymeric radical, exhibit reactivity that can be as much as 50–100 times greater than if those same pendant vinyl groups were homogeneously distributed throughout the polymerizing mixture.[34,53,137] Unfortunately, the strong spatial correlations that lead to the enhanced reactivity also lead to the consumption of these potential crosslinks by the relatively ineffective reaction that forms primary cycles, ultimately leading to the formation of what has classically been referred to as "microgels" or internally crosslinked polymers.[34,77,137–140]

At the earliest stages of the polymerization, before macrogelation, microgels exist as independent regions of high crosslink density in a monomer pool. As the polymerization proceeds, microgels continue to form and their growth ultimately leads to macrogelation of the polymer, though at higher conversions than predicted classically due to cyclization. As the polymerization proceeds, the reactive radical centers continue to display a strong propensity for intramolecular crosslinking, which dramatically reduces the mobility of the radicals within the nanoscale regions where the radicals exist. Radicals are ultimately trapped within regions of high crosslink density and unable to continue to propagate, thus leading to an effective unimolecular mechanism for termination of the radical activity.[34,68] At the completion of the polymerization, the final network structure is one of the highly crosslinked regions, containing trapped radicals surrounded by less densely crosslinked regions that contain a disproportionate amount of unreacted monomer.[54]

Modeling heterogeneity

Modeling of crosslinked polymer networks was pioneered by the seminal work of Flory[141] and Stockmayer,[142] providing a mathematical framework that pervades all modern statistical polymerization models today. Despite the success of this mean-field model, cyclization was not originally included, leading to the discrepancies between theoretical predictions and experimental observations such as the location of the gel-point conversion. Modern statistical models have incorporated weak cyclization as well as unequal reactivity of chemical moieties, predicting significant microgel formation within 1% of the polymerization[53]; however, such models fail to predict many nuances that manifest structural heterogeneity and propagate throughout the various stages of polymerization, particularly in polymerizations that incorporate higher levels of crosslinking agents as typical in photopolymerization reactions.

One highly successful route to modeling the primary cyclization reaction utilizes an approach that incorporates species balances for pendant vinyl groups formed at any stage during the polymerization.[64,65,143,144] This approach is unique in that it develops and solves the differential kinetic equations accounting for the reactivity difference of the pendant double bonds spatially and throughout the polymerization. Monomeric and pendant double bonds are tracked separately to capture the local dynamics and reactivity of the pendant double bonds. Calculation of the consumption rate of monomeric double bonds is based on mean field kinetics for both the monomer species and the radicals, whereas for pendant dou-

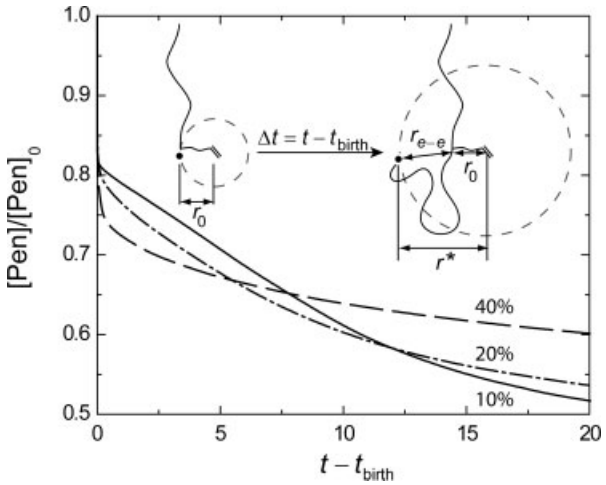

Figure 13. Predictions for the normalized fraction of pendant vinyl groups that were formed at 10% (solid line), 20% (dot-dashed line), and 40% (dashed) conversion that remain unreacted as a function of time since the moiety was created (i.e., t_{birth}).

As illustrated in the figure inset, the distance from the active center to the pendant vinyl group increases as a function of $t - t_{birth}$, scaling approximately with end-to-end length, r_{e-e}, to the 1/2 power, and decreasing the reactivity of the pendant vinyl group for primary cyclization. Figure adapted from refs. 146 and 145.

ble bonds, consumption is associated with both crosslinking (mean-field) and primary cyclization (by back-biting of the same radical that reacted with the initial monomer). For the primary cyclization reaction, a local radical concentration is determined based on the distance between the terminal radical and each pendant vinyl group on the polymer chain, as illustrated within Figure 13. The resulting expression for the total pendant consumption rate is

$$R_{pen}(t) = k_{xl}[\mathrm{Pen}(t)][R_b] + \frac{k_{cyc}}{N_A}\sum_{t_b=0}^{t_b=t}\frac{\exp\{-k_t[R_b](t-t_b)\}[\mathrm{Pen}(t-t_b)]}{\frac{4}{3}\pi\left(r_0 + C_n^{1/2}n(t,t_b)^{1/2}l\right)^3}, \quad (7)$$

where the kinetic constants for propagation that lead to crosslinking and cyclization are k_{xl} and k_{cyc}, respectively, which are both generally assumed to be equal to k_p, the propagation kinetic constant. $[R_b]$ is the bulk radical concentration, N_A is Avogadro's number, r_0 is the monomer size, C_n is the characteristic ratio, n is the number of carbon–carbon bonds between the pendant double bond and radical, and l is the length of a carbon–carbon bond. Clearly, pendant double bonds that have existed for different lengths of time each have their own local radical concentration, which is a function of when the pendant was created (birth time, t_b) and the current time, t. When the pendant is first created, it is very close to the propagating radical and the local radical concentration (and therefore the rate of primary cycle formation as indicated by the second term in Eq. 7) is high. Conversely, after long times the local radical concentration diminishes dramatically and the crosslinking reaction dominates the reactivity. The effect of various reaction parameters on the pendant vinyl reactivity and propensity to form crosslinks is presented in Figure 13. This approach has been highly successful in predicting the deviation of the crosslink density from ideality as a function of monomer structure,[65] monomer size,[143] crosslinking agent functionality,[64] and the presence of varying amounts and qualities of solvent.[146]

Despite its success in predicting the decrease in the average crosslinking density associated with primary cyclization, analytical models have struggled to predict the spatial distribution of crosslinking density. In contrast, Monte Carlo based computer simulations have been able to capture the heterogeneous structural evolution and spatial variations in crosslink density. Percolation or kinetic gelation-type simulations elucidate the dependence on polymerization conditions of a number of characteristics of highly crosslinked networks such as microgel formation,[140] monomer pooling,[140] radical trapping,[76] and delayed gelation.[137] The reactivity ratio of pendant vinyl groups to free monomer vinyl group demonstrates a reactivity decrease over the simulation, starting from values as large as 50, and dropping below unity.[139] In these simulations, the observed reactivity preference for pendant vinyl groups is strictly a function of spatial distribution and mobility as observed experimentally. Interestingly, the inversion to lower reactivity later in the polymerization is due to the trapping of "older" pendant vinyl groups within the microgels formed at the early stages of the polymerization.

Iniferter photopolymerizations and material properties

As discussed previously, structural heterogeneity in highly crosslinked networks is marked by regions of dramatically different mobility. Time-dependent properties, such as the stress and dielectric[56] relaxation, reflect the underlying molecular relaxation, revealing the relaxation time distribution associated with this heterogeneity. Dynamic mechanical analysis and dielectric analysis were both used to characterize the heterogeneous relaxation time distribution in polymer networks.[56,57,147]

Unfortunately, significant complications arise when attempting to characterize the structural heterogeneity of highly crosslinked networks by any technique that requires a temperature ramp.[55] Trapped radicals readily exist for months to years within the highly crosslinked, glassy polymer matrix.[34] As the temperature is increased during any attempted evaluation of the material properties, the radical mobility increases, facilitating further propagation with the remaining vinyl groups. This process, known as chasing, previously was intractable as it shifts the glass transition temperature of the sample while the same is being measured, resulting in an inaccurate measurement. One mitigation strategy is to scan multiple times; however, the final material measurement is on a sample that is chemically far different from the original. Thus, measurements by this technique superimpose the network properties from the initial photopolymerization with the subsequent thermal polymerization. An alternative strategy developed first by our group is to use iniferters to facilitate radical termination and elimination of trapped radicals before the necessary temperature excursion.

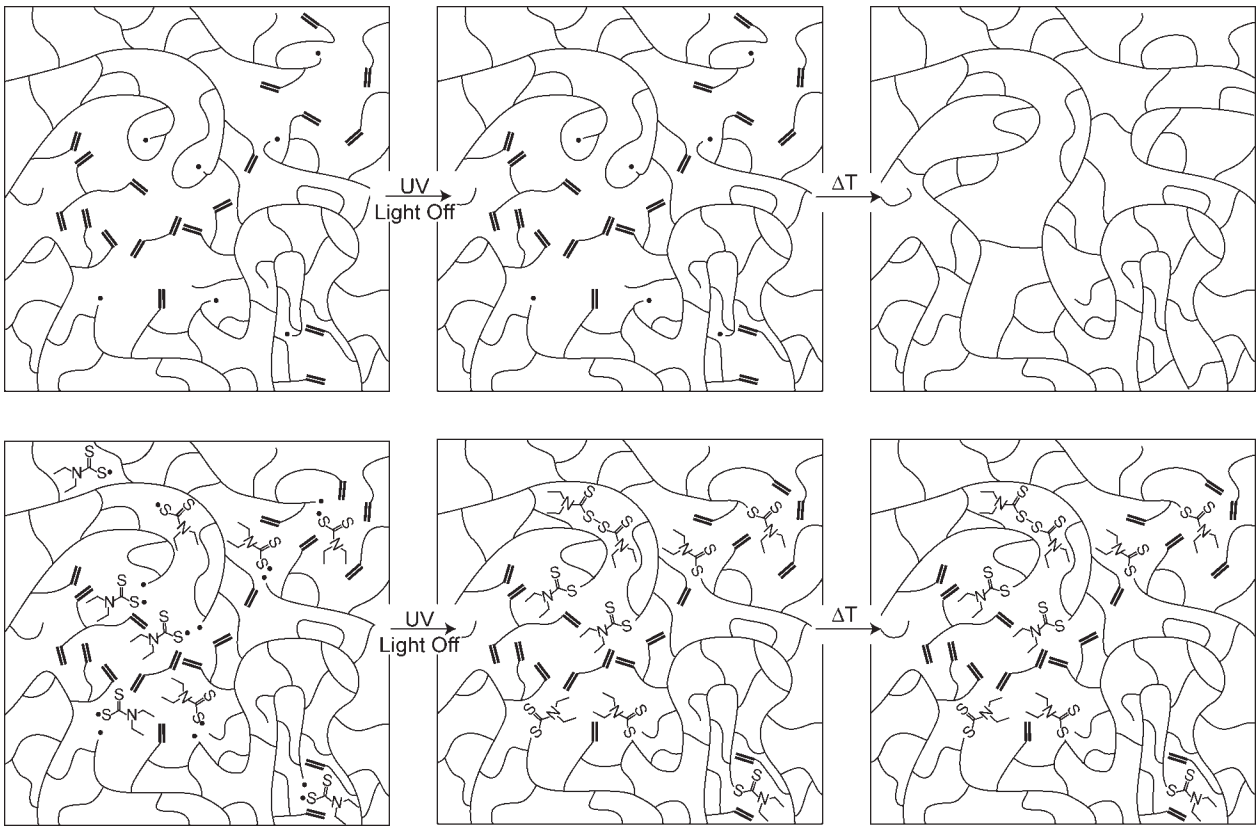

Figure 14. Conventional (top) and iniferter mediated (bottom) polymerization of highly crosslinked networks.

After the irradiation has ceased in the iniferter photopolymerization, the stable radicals sequester the active carbon-centered radicals, preventing further polymerization during heating. Adapted from ref. 55.

Iniferters were first used to synthesize several polymer architectures including block copolymers,[148] graft copolymers,[149] star polymers,[150] and low polydispersity linear polymers.[151,152] Ideally, an iniferter is photocleaved to form an initiating radical and a stable, noninitiating radical. Because this latter radical does not initiate polymerization, it remains small and relatively mobile throughout the polymerization reaction. Thus, when irradiation ceases, the small, stable, and noninitiating radical is capable of diffusing throughout the polymer and terminating the carbon-centered radicals, including the otherwise trapped radicals. This mechanism, as illustrated in Figure 14, thus prevents the phenomenon of chasing upon subsequent heating and enables a far more accurate and comprehensive analysis of the polymer networks formed from photopolymerizations.

Figure 15 shows the reversible photo-cleavage of the iniferter, *p*-xylylene bis(*N*,*N*-diethyl dithiocarbamate) (XDT) into a xylyl radical, which initiates polymerization, and two stable dithiocarbamyl (DTC) radicals, maintaining an equilibrium with the carbon centered radical as a function of irradiation wavelength and intensity. When the irradiation is ceased, the otherwise trapped radicals become quenched by the DTC radicals, thus preventing further polymerization upon heating (as shown in Figure 14). Traditional photocleavable radical initiators can also be used in conjunction with a sufficient amount of tetraethylthiuram disulfide (disulfide-DTC or TED) to achieve a similar outcome but with enhanced capabilities.[153] This approach has the advantage of independent control of the two radical species concentrations and is appropriate for creating networks that polymerize rapidly but still contain DTC end groups as needed for multilayer device manufacture and photografting reactions.[4,154,155]

It is important to note that the introduction of stable, noninitiating radical species, such as DTC, changes the overall reaction mechanism and the corresponding polymerization rate. Early in the polymerization, there are low concentrations of DTC species and the dominant termination mode is by reaction of two carbon–carbon radicals. Later in the polymerization, there is a build up of DTC radicals and the dominant termination mode shifts to the combination of carbon and DTC radicals. Using XDT in conjunction with TED, Kannurpatti et al. were able to characterize these polymeriza-

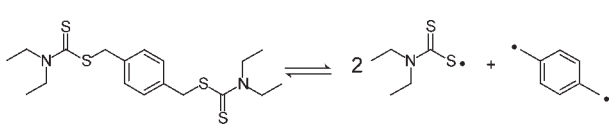

Figure 15. Upon irradiation of UV light, XDT (left) undergoes reversible photocleavage of the carbon-sulfur bond to produce two propagating carbon centered radicals (far right) and two nonpropagating DTC radicals.

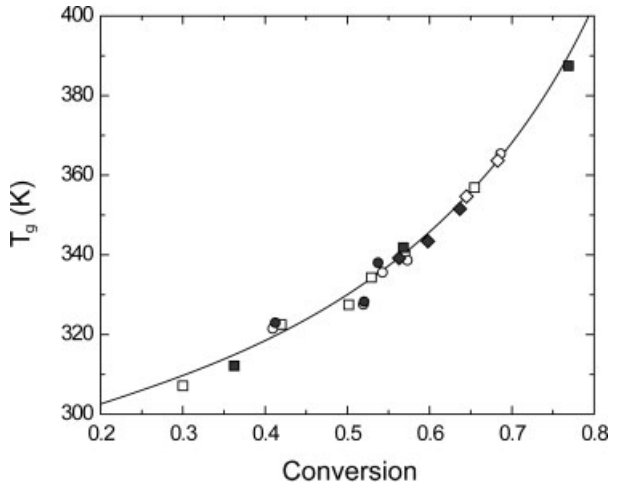

Figure 16. The glass transition temperature of a 75/25 mixture of 2,2-*bis*[4-(2-hydroxy-3-methacryloxyprop-1-oxy) phenyl] propane (*bis*-GMA) and triethylene glycol dimethacrylate.

Irradiating intensity ranged from as low as 0.05–800 mW/cm^2, for samples formulated with 0.1 wt% XDT. Further, data were collected for samples polymerized at temperatures ranging from 10 to 70°C. These results clearly demonstrate that for highly crosslinked polymer systems the initiation rate and polymerization conditions primarily dictate the final conversion as a means for altering the material properties. Figure adapted from ref. 75.

tion stages and found a regime where carbon-DTC radical termination dominates throughout the reaction, establishing a "living" network polymerization.[98]

The application of XDT in a divinyl polymerization not only prevents the chasing phenomenon associated with trapped radicals but also prevents "dark" polymerization, that is, continued polymerization after irradiation has ceased. Typically, it is difficult to measure the evolution of mechanical properties at specific conversions due to this dark polymerization. Figure 16 demonstrates the use of iniferters for conversion control and evaluation of the evolution of the glass transition temperature for a typical dental resin composed of two dimethacrylates. Here, it is clear that, despite several orders of magnitude change in the initiation rate as well as a large change in the polymerization temperature, the glass transition temperature of this complex system is determined only by the conversion that is achieved. Several other properties were also evaluated (modulus, strength, etc.) and found to depend only on conversion rather than the initiation conditions.[75,156,157] These results indicate that the "soft-start" and other ramped curing methodologies used in dental applications primarily alter the functional group conversion rather than changing the relationship between conversion and material properties.

Time-temperature superposition (TTS) is applicable only to materials that do not undergo a phase transition or chemical reaction over the temperature range used. Figure 17 shows the storage modulus as a function of frequency for a copolymerized network of diethylene glycol dimethacrylate (DEGDMA) and poly(ethylene glycol 600) dimethacrylate (PEG600DMA), revealing a broad glass transition owing to the structural heterogeneity. Without the application of iniferters, TTS would be impossible as the material would be chemically different at each temperature. This result also quantitatively presents the dramatic structural heterogeneity that exists in these materials as the transition from glassy to rubbery occurs over as many as 15–18 orders of magnitude in relaxation time.

To characterize the sample heterogeneity in terms of a single, lumped parameter, the relaxation spectrum is often fit to a stretched exponential or Kohlrausch-Williams-Watts (KWW) function, $\exp[-(\omega_c/\omega)^{\beta}]$.[158] Perfectly, homogeneous materials relax by a single relaxation mode and are well described by a simple exponential ($\beta = 1$), whereas heterogeneous materials relax by the superposition of relaxation modes, convoluting the response and "stretching" the decay ($0 < \beta < 1$). Thus, the distribution parameter, β, is a measure of homogeneity. In Figure 18, the distribution parameter was measured for copolymerizations of octyl methacrylate (OcMA, a noncrosslinking monomethacrylate) with one of two crosslinking agents, either DEGDMA or PEG600DMA. The primary difference between the two dimethacrylate crosslinking agents is the molecular size, corresponding to the distance between the vinyl functionalities. Interestingly, as one increases the amount of dimethacrylate comonomer, the smaller DEGDMA is more heterogeneous, with a lower distribution parameter, than the larger PEG600DMA. This outcome is explained in terms of primary cyclization, where the pendant vinyl groups are more likely to cyclize in the shorter monomer, leading to the formation of a more uniform network from PEG600DMA when compared with DEGDMA. This picture is consistent with both theoretical models[146,145] and kinetic gelation simulations.[137]

Adaptable Networks

Chemically crosslinked networks are generally described as thermosets, in recognition that these networks can be nei-

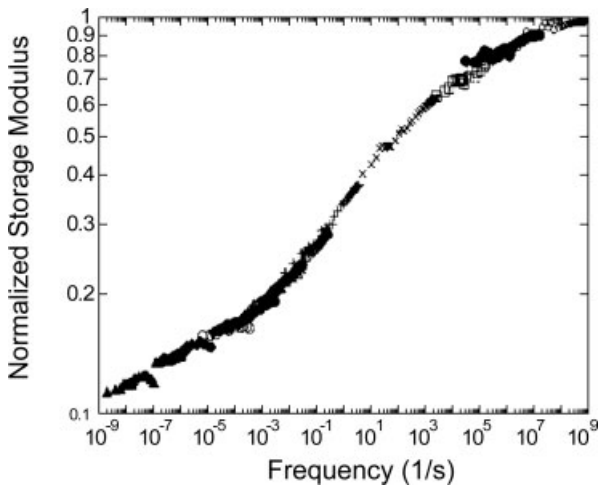

Figure 17. Storage modulus for a 45/55 wt/wt, DEGDMA/PEG600DMA copolymer, over 18 decades of frequency using time-temperature superposition (temperatures are from −37.7°C to 121.7°C).

Figure adapted from ref. 55.

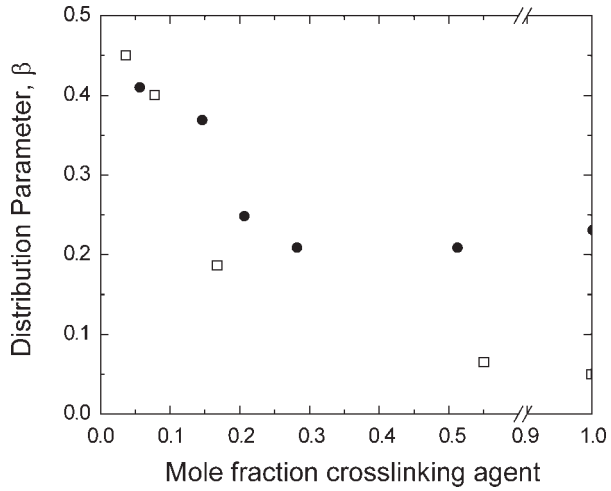

Figure 18. Distribution parameter versus mole fraction crosslinking agent in copolymers of (□) OcMA and DEGDMA and (●) OcMA and PEG600DMA.

All samples were formulated with 0.1 wt % XDT and irradiated 365 nm light at 600 mW/cm^2. Figure adapted from ref. 57.

ther melted nor molded. Recently, we have developed a new class of materials, known as "adaptable networks," which implement covalent but reversible chemical linkages throughout the network backbone, which facilitates controllable bond rearrangement and material reshaping. These new materials impact several areas of polymerization as they provide a mechanism for postgelation stress relief and even reverse material failure through crack healing. Our approach has been to implement photoinduced network rearrangement via addition-fragmentation of an allylic sulfide group within a crosslinked polymer backbone.

When incorporated throughout a network, the allylic sulfide functionality has the ability to undergo radical mediated addition-fragmentation (i.e., intramolecular hydrolytic substitution, S_H2')[159,160] and has been utilized in a variety of synthetic schemes,[161,162] including methods for synthesizing low-polydispersity linear polymers.[163–165] The allylic sulfide moiety is a rather poor reversible addition-fragmentation chain transfer (RAFT) agent with respect to carbon-centered radicals[163]; conversely, it readily reacts with thiyl radicals generated within the thiol-ene polymerization chemistry (Figure 19). Interestingly, the reaction between the thiyl radical and the allylic sulfide bond regenerates the reactants, resulting in bond rearrangement while preserving the overall network structure and crosslinking density. This bond rearrangement has been shown to enable photoactuation and stress relaxation, each associated with adapting/relaxing all or part of the polymer network.

There are several strategies to incorporate the allylic sulfide functionality within the network backbone. Ring opening monomers, such as monomer I in Figure 20, are implemented directly into a stoichiometrically balanced ratio of thiols to enes, whereas the amount of allyllic sulfide within the network is readily controlled. This method decreases the crosslink density and produces a distribution of allylic sulfide

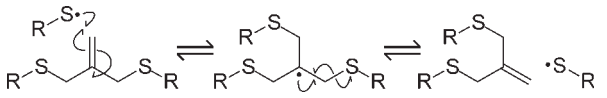

Figure 19. Addition-fragmentation mechanism for the thiyl radical attack on an allylic sulfide moiety.

This mechanism facilitates macroscopic shape changes and material relaxation; however, the network connectivity, overall crosslink density, and material properties are all conserved as one crosslink or backbone connection is simply exchanged for a new connection.

units per crosslink, which is dependent on the allylic sulfide reactivity relative to the "ene" reactivity. An alternative method is to synthesize one of the thiol-ene monomers with an allylic sulfide unit (e.g., monomer II in Figure 20). Although this guarantees one allylic sulfide unit per one crosslink, the amount of allylic sulfide units is fixed. The combination of the two monomers provides facile control over the amount of allylic sulfide units per crosslink.

A typical resin formulation includes both a visible- (e.g., bis(2,4,6-trimethylbenzoyl)-phenylphosphineoxide) and UV-light initiator (e.g., 1-hydroxy-cyclohexyl-phenyl-ketone). The resin is photopolymerized using 400–500 nm visible-light, leaving latent UV-light initiator for subsequent radical generation and stress relaxation via bond rearrangement. Figure 21a demonstrates the stress profile of a material stretched to various strains, showing an elastic linear response to the deformation. After reaching the prescribed strain, the material was irradiated with UV-light. Normalization of the data reveals that approximately 90% of the stress is relieved upon irradiation, owing to photoinduced plastic deformation via bond rearrangement as mediated by the allylic sulfides (see Figure 21b).

Because the addition-fragmentation of the thiol-ene allylic sulfide linkage is triggered by an external light source, the bond rearrangement within these networks is both spatially and temporally controlled. Irradiation of optically thick samples under tensile stress results in light attenuation, essentially "writing" a gradient of stress into the material that mimics the light intensity gradient. After removal from the tensile stress, the material deforms in response to the written stress gradient.[135] Moreover, the written stress gradient can be altered further by additional irradiation, producing light-induced actuation of the material.[136] Adaptable networks are still in the nascent stages of development; however, this exciting new branch of materials exhibits photoinduced plasticity, as displayed in thiol-ene allylic sulfide networks,

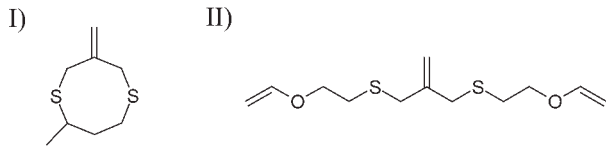

Figure 20. Chemical Structures for I) 2-methyl-7-methylene-1,5-dithiacyclooctane (MDTO) and II) 2-methylene-propane-1,3-di(thioethyl vinyl ether) (MDTVE).

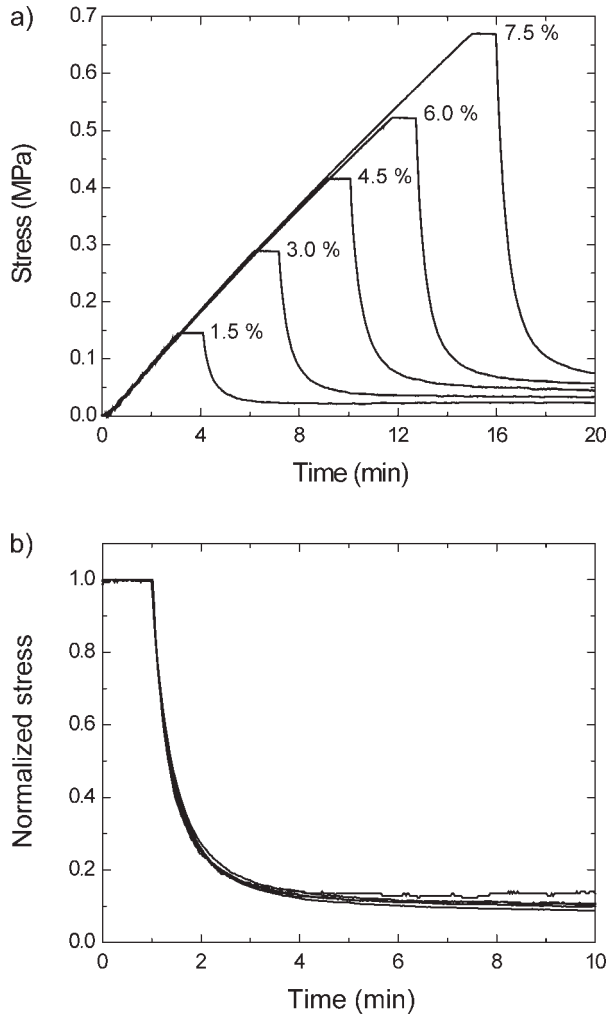

Figure 21. (a) Stress vs. time and (b) normalized stress versus time for samples of 75% PETMP/MDTVE and 25% MDTO ramped to 1.5, 3.0, 4.5, 6.0, and 7.5% strain at 0.5%/min, held for 1 min, and irradiated with 365 nm light at an intensity of 40 mW/cm^2.

The normalized stress versus time reveals that 90% of the stress is alleviated upon irradiation nearly independent of the initial strain.

allowing for precise control over the shape as well as actuation.

Photopolymerization Reaction Engineering for Novel Applications Development

Dental materials

Until recently, most dental restorations were completed with materials based on metal amalgams. In contrast, methacrylate based resins have the added aesthetically pleasing benefit of being camouflaged within the tooth; however, they have been limited by the mechanical properties achieved, including a large stress associated with the polymerization shrinkage and simultaneous polymer network formation. Today, visible-light initiated, dimethacrylate-based resins are the most commonly used material for dental restoration.[10] Despite incremental advancements, dental resins still face fundamental obstacles associated with rapid chain-growth photopolymerization, such as incomplete conversion, and stress development due to polymerization-induced volume shrinkage.

Incomplete conversion of highly crosslinked monomers in dental restorative materials is an unresolved problem, where double bond conversion in a typical dental resin is 55 to 75%.[166–168] Low double bond conversion equates to unreacted monomer that not only diminishes the mechanical properties via plasticization but also can leach out of the restoration and into the body. Several parameters can be manipulated to dictate the final conversion such as light intensity, reaction temperature, monomer structures, and composition; these parameters determine the diffusional limitations on termination (autoacceleration) in the initial stages of the reaction and the subsequent diffusional limitation to propagation (autodeceleration) in the latter stages of the reaction.[156]

Recently, the focus of the dental community has aimed at reducing or eliminating the shrinkage stress that arises during the polymerization. These stresses, frequently topping 1–3 MPa, are large enough to deform the tooth structure measurably and cause marginal leaking, microcracking, sensitization, and, ultimately, secondary cavities at the site of the original cavity.[10] The dental community experimented with irradiation intensity and timing as a means for achieving reduced stress, and various curing protocols emerged as a result, reporting lower polymerization stress associated with lower intensity, "soft-start" protocols. Ultimately, these claims were confounded by the failure to account for the relationship between the double bond conversion, the initiation conditions, and the observed polymerization stress. Lu et al. performed the first simultaneous stress and conversion measurements and demonstrated that the low intensity protocol did indeed result in lower polymerization stress, but at the price of having a lower double bond conversion (see Figure 22).[9,32]

Though the soft-start methodologies achieved little practical success in stress reduction, there have been many strategies successfully used over the years to reduce polymerization shrinkage and the associated stress. The most successful of these approaches has been to simply reduce the monomer volume fraction and replace it with nonshrinking inorganic fillers such as silica particles. The current research focus is on minimizing the shrinkage in the organic fraction without sacrificing reaction speed or mechanical properties. Although Patel et al.[169] established a direct relationship between volume shrinkage and carbon–carbon double bond conversion for methacrylates, several researchers have circumvented this limitation by ring-opening polymerizations, which exhibit less shrinkage.[170–174]

As mentioned, thiol-ene photopolymerizations proceed via a free-radical step-growth mechanism and exhibit a much reduced volume shrinkage per double bond converted (~12.5 ml/mol).[8] Further, the molecular weight of thiol-ene step-growth polymerizations increases geometrically and uniformly, imparting pregel characteristics that are particularly well suited for application in dental materials and delaying the gel-point conversion until much higher conversions, when compared with typical chain-growth photopolymerizations. Small molecular species dominate the initial polymerization stages, allowing shrinkage stress dissipation through

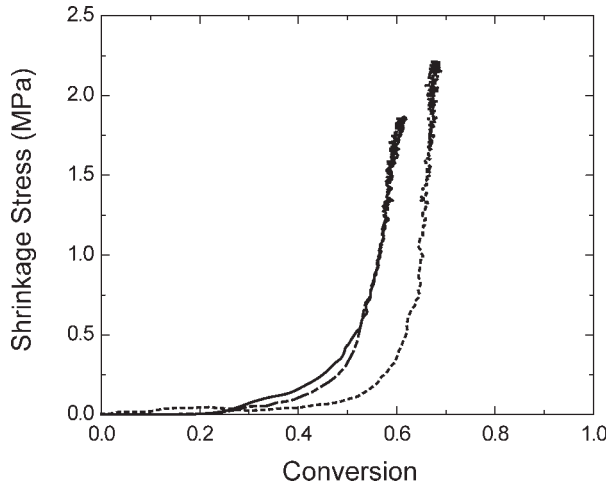

Figure 22. The stress evolution of a typical filled dental resin (49/21/30 — 2,2-*bis*[4-(2-hydroxy-3-methacryloxyprop-1-oxy) phenyl] propane (bis-GMA)/triethylene glycol dimethacrylate (TEGDMA)/OX-50) using three different curing protocols: Standard-start (dotted line — 60 seconds at 450 mW/cm^2), Soft-start (solid line — standard-start protocol preceded by 5 s at 100 mW/cm^2), Pulse-start (dashed line — same as soft-start with a 120 s wait period between the 5 and 60 s irradiation period).

All samples were formulated with 0.21 wt % camphorquinone and 0.56 wt % 4-dimethylaminobenzoate and were irradiated with visible light. Figure adapted from ref. 9.

viscous flow. This behavior is in contrast to chain-growth polymerizations, where large molecular species are generated shortly after initiation, with a gel-point conversion typically less than five percent. Figure 23 presents results for a thiol-ene formulation in contrast to the traditional dental resin system, where the thiol-ene polymerization achieves higher conversions, resists oxygen inhibition, and exhibits significantly lower stresses.

Hydrogels

Biomaterial research is a rapidly expanding multidisciplinary field that focuses on the interplay between materials and biological systems. An important class of biomaterials is the insoluble, yet hydrated networks called hydrogels. Hydrogels are readily tailored and used in a variety of applications such as contact lenses, super-absorbent materials, and adhesives.[11,13,175] The polymer strands that comprise the hydrogel network control the extent of swelling and dictate the mechanical properties. Incorporation of hydrolytically degradable units such as ester or anhydride functionality into the network backbone or crosslinks provides an avenue for hydrogel dissolution in the presence of water. Hydrolytically degradable hydrogels have been integrated into many applications such as degradable sutures and stents, tissue engineering matrices, and sustained drug delivery devices.[176–182]

To be a useful biomaterial, hydrogels and their degradation products must be biocompatible and degradation must occur in a controlled and consistent manner. It is essential to have an accurate model to predict the erosion evolution of a hydrogel to exploit the degradation properties for a specific application. A statistical model was constructed to predict the bulk-erosion of a poly(ethylene glycol)-*block*-poly(lactic acid)-*block*-poly(ethylene glycol) (PEG-*b*-PLA-*b*-PEG) backbone hydrogel.[180] The PEG block imparts hydrophilic solubility to an otherwise hydrophobic, yet hydrolytically cleavable, PLA block. The basic tradeoffs between mechanical strength and water content are observed as a function of the molecular weight between crosslinks and the composition. The basic degradation of a single hydrolytic linkage is simply described using first or pseudo-first order kinetics. Using the single adjustable parameter of the number of crosslinks per kinetic chain, one predicts the resulting mass loss profile.[180] Simple modifications to the model, such as the inclusion of dangling ends (i.e., chains not fully incorporated into the network), multiple degradable units per hydrolytic chain, and chain-length distributions, lead to a more accurate description of the degradation.[183] Figure 24 shows a comparison of the mass loss model with and without the incorporation of dangling ends.

Microfluidic devices

Over the last decade, microfluidic devices have become increasingly popular with the main goal being the production of comprehensive laboratory analysis and detection systems on a single, self-contained microdevice. This device should successfully reduce macroscale technologies and analytical

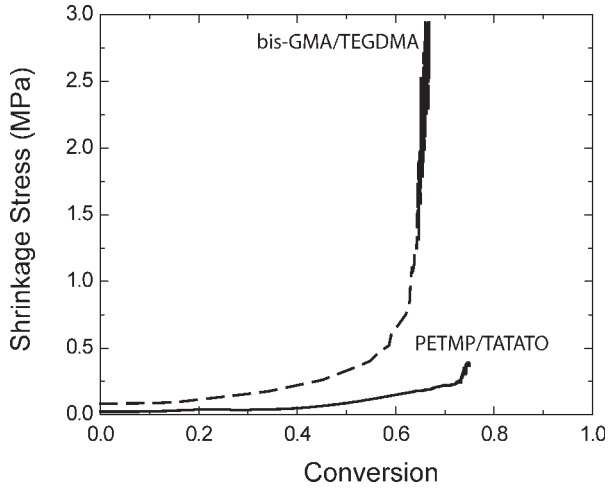

Figure 23. The stress evolution of a typical dental resin formulation (70/30 — 2,2-*bis*[4-(2-hydroxy-3-methacryloxyprop-1-oxy) phenyl] propane (*bis*-GMA) and triethylene glycol dimethacrylate (TEGDMA), dashed line) and a stoichiometrically balanced thiol-ene formulation (pentaerythritol tetrakis(3-mercaptopropionate) (PETMP)/Triallyl-1,3,5-Triazine-2,4,6-Trione (TATATO), solid line).

All samples were formulated with 0.3 wt % camphorquinone and 0.8 wt % 4-dimethylaminobenzoate and were irradiated with visible light at 580 mW/cm^2 for 1 min. Figure adapted from ref. 8.

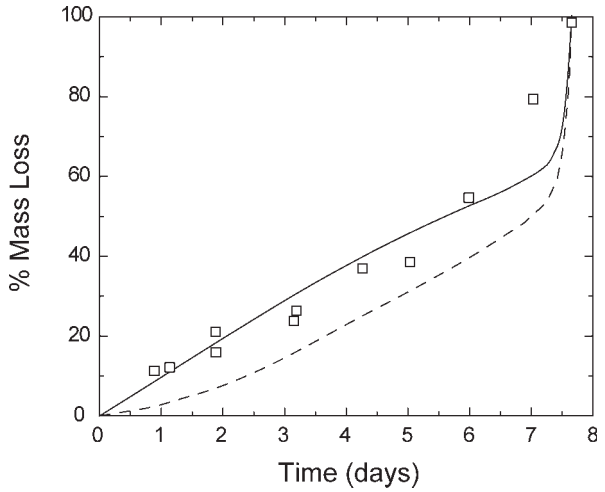

Figure 24. Experimental mass loss versus time (□) for a 4600-5.6 PLA-b-PEG-b-PLA hydrogel comparing a statistical model with (solid line) and without (dashed line) the consideration of chain dangling ends.

Figure adapted from ref. 183.

functions to a microscale, be robust in the operating conditions that are tolerated, be as affordable as possible to produce, and be as simple as possible to use. Microfluidic device technology, as such, has many advantages, requiring reduced sample sizes, producing results more rapidly and accurately, and facilitating the use of field portable systems. Photopolymerization techniques are ideally suited to this complex device development in many areas. Our research in particular has developed the contact liquid photopolymerization process to take advantage of iniferter polymerizations for the fabrication of complex, three-dimensional devices.[4,5] This technique provides excellent adhesion between layers, preventing delamination, and a strategy for grafting monomers that alter surface energy to either prevent or encourage biological interactions[154,155] as well as functionalized antibodies to facilitate rapid detection.[184–186] Improved antigen detection is achieved by copolymerizing methacrylated antibodies with PEG methacrylate from the surface graft. The PEG methacrylate imparts significant mobility and hydration, which eliminates both mass transfer and steric limitations to the antigen-antibody interaction, thereby improving the kinetics and facilitating highly sensitive, rapid detection that would otherwise not be achievable.

Biosensing

Ultrasensitive detection of biological moieties is an excellent illustration of a nonconventional application of photopolymerization reactions.[187–189] For this work, photoinitiators were coupled to molecules involved in biorecognition events such as antigen-antibody interactions or oligonucleotide hybridization reactions. Upon photopolymerization, macroscopic polymer spots, observable to the naked eye, were formed from $\sim 10^3$ biological moieties (biotin-labeled DNA in this case) at a surface density of less than 0.1 biotin/μm^2. This sensitivity was achieved without enzymatic amplification or detection schemes, and it portends to the great ability of polymerization reactions to serve a critical role in biodetection as applied to disease diagnosis, biowarfare agent detection, and genetic fingerprinting.

Conclusions

The photopolymerization reaction is a highly versatile and capable reaction; yet it remains one of the least understood and implemented due to the complexity of the rapidly evolving network structure, the mass and heat transfer limitations, and the lack of availability of custom, functional monomers. Over the last 15 years, our group has attempted to address these issues by a combination of fundamental reaction engineering principles and network modeling as well as thorough experimental validation of that understanding and the underlying formation-structure-property relationships. Further, we have exploited unique polymerization schemes as well as the development of novel materials to enable new and improved application of photopolymerization technologies.

Acknowledgments

CNB would like to recognize the exceptional contributions of his undergraduate and graduate students, postdoctoral associates and faculty, and industrial colleagues, each of whom has contributed immensely to and is responsible for this work. Each of these individuals has been of the highest quality and ability. Further, continuing financial support from the National Institutes of Health (through grant #DE10959 as well as several others), the National Science Foundation (through a Presidential Faculty Fellowship as well as others), the Industry/University Center for Fundamentals, and Applications of Photopolymerizations, as well as many others are acknowledged.

Literature Cited

1. Decker C. Uv-curing chemistry—Past, present, and future. *J Coating Technol*. 1987;59:97–106.
2. Anseth KS, Newman SM, Bowman CN. Polymeric dental composites: properties and reaction behavior of multimethacrylate dental restorations. In: *Biopolymers Ii*, Vol. 122. Berlin 33: Springer-Verlag, 1995:177–217.
3. Berchtold KA, Nie J, Stansbury JW, Hacioglu B, Beckel ER, Bowman CN. Novel monovinyl methacrylic monomers containing secondary functionality for ultrarapid polymerization: steady-state evaluation. *Macromolecules*. 2004;37:3165–3179.
4. Hutchison JB, Haraldsson KT, Good BT, Sebra RP, Luo N, Anseth KS, Bowman CN. Robust polymer microfluidic device fabrication via contact liquid photolithographic polymerization (CLiPP). *Lab Chip*. 2004;4:658–662.
5. Haraldsson KT, Hutchison JB, Sebra RP, Good BT, Anseth KS, Bowman CN. 3D polymeric microfluidic device fabrication via contact liquid photolithographic polymerization (CLiPP). *Sensor Actuator B Chem*. 2006;113:454–460.
6. Johnson PM, Reynolds TB, Stansbury JW, Bowman CN. High throughput kinetic analysis of photopolymer conversion using composition and exposure time gradients. *Polymer*. 2005;46:3300–3306.
7. Lovell LG, Berchtold KA, Elliott JE, Lu H, Bowman CN. Understanding the kinetics and network formation of dimethacrylate dental resins. *Polymer Adv Tech*. 2001;12:335–345.
8. Lu H, Carioscia JA, Stansbury JW, Bowman CN. Investigations of step-growth thiolene polymerizations for novel dental restoratives. *Dent Mater*. 2005;21:1129–1136.
9. Lu H, Stansbury JW, Bowman CN. Impact of curing protocol on conversion and shrinkage stress. *J Dent Res*. 2005;84:822–826.
10. Stansbury JW, Bowman CN, Newman SM. Shining a light on dental composite restoratives. *Phys Today*. 2008;61:82–83.
11. Wichterle O, Lim D. Hydrophilic gels for biological use. *Nature*. 1960;185:117–118.

12. Zwiers RJM, Dortant GCM. Aspherical lenses produced by a fast high-precision replication process using uv-curable coatings. *Appl Optic*. 1985;24:4483–4488.
13. McMahon TT, Zadnik K. Twenty-five years of contact lenses—The impact on the cornea and ophthalmic practice. *Cornea*. 2000;19:730–740.
14. Ma HM, Davis RH, Bowman CN. A novel sequential photoinduced living graft polymerization. *Macromolecules*. 2000;33:331–335.
15. Harant AW, Khire VS, Thibodaux MS, Bowman CN. Thiol-ene photopolymer grafts on functionalized glass and silicon surfaces. *Macromolecules*. 2006;39:1461–1466.
16. Khire VS, Harant AW, Watkins AW, Anseth KS, Bowman CN. Ultrathin patterned polymer films on surfaces using thiol-ene polymerizations. *Macromolecules*. 2006;39:5081–5086.
17. Khire VS, Lee TY, Bowman CN. Surface modification using thiol-acrylate conjugate addition reactions. *Macromolecules*. 2007;40: 5669–5677.
18. Willson CG, Trinque BC. The evolution of materials for the photolithographic process. *J Photopolym Sci Technol*. 2003;16:621–627.
19. Gates BD, Xu QB, Stewart M, Ryan D, Willson CG, Whitesides GM. New approaches to nanofabrication: molding, printing, and other techniques. *Chem Rev*. 2005;105:1171–1196.
20. Khire VS, Yi Y, Clark NA, Bowman CN. Formation and surface modification of nanopatterned thiol-ene substrates using step and flash imprint lithography. *Adv Mater*. 2008;20:3308–3313.
21. Beebe DJ, Moore JS, Bauer JM, Yu Q, Liu RH, Devadoss C, Jo BH. Functional hydrogel structures for autonomous flow control inside microfluidic channels. *Nature*. 2000;404:588–590.
22. Luo N, Hutchison JB, Anseth KS, Bowman CN. Synthesis of a novel methacrylic monomer iniferter and its application in surface photografting on crosslinked polymer substrates. *J Polym Sci Part A: Polym Chem*. 2002;40:1885–1891.
23. Luo N, Hutchison JB, Anseth KS, Bowman CN. Surface-initiated photopolymerization of poly(ethylene glycol) methyl ether methacrylate on a diethyldithiocarbamate-mediated polymer substrate. *Macromolecules*. 2002;35:2487–2493.
24. Luo N, Metters AT, Hutchison JB, Bowman CN, Anseth KS. A methacrylated photoiniferter as a chemical basis for microlithography: micropatterning based on photografting polymerization. *Macromolecules*. 2003;36:6739–6745.
25. Anseth KS, Metters AT, Bryant SJ, Martens PJ, Elisseeff JH, Bowman CN. In situ forming degradable networks and their application in tissue engineering and drug delivery. *J Controlled Release*. 2002;78:199–209.
26. Rydholm AE, Bowman CN, Anseth KS. Degradable thiol-acrylate photopolymers: polymerization and degradation behavior of an in situ forming biomaterial. *Biomaterials*. 2005;26:4495–4506.
27. Rydholm AE, Anseth KS, Bowman CN. Effects of neighboring sulfides and pH on ester hydrolysis in thiol-acrylate photopolymers. *Acta Biomaterialia*. 2007;3:449–455.
28. Neckers DC. Architecture with photopolymerization. *Polym Eng Sci*. 1992;32:1481–1489.
29. Young JS, Fox SR, Anseth KS. A novel device for producing three-dimensional objects. *J Manuf Sci Eng-Trans Asme*. 1999; 121:474–477.
30. Francis LF, McCormick AV, Vaessen DM, Payne JA. Development and measurement of stress in polymer coatings. *J Mater Sci*. 2002;37:4897–4911.
31. Lu H, Stansbury JW, Dickens SH, Eichmiller FC, Bowman CN. Probing the origins and control of shrinkage stress in dental resin-composites. I. Shrinkage stress characterization technique. *J Mater Sci-Mater Med*. 2004;15:1097–1103.
32. Lu H, Stansbury JW, Bowman CN. Towards the elucidation of shrinkage stress development and relaxation in dental composites. *Dent Mater*. 2004;20:979–986.
33. Braga RR, Ballester RY, Ferracane JL. Factors involved in the development of polymerization shrinkage stress in resin-composites: a systematic review. *Dent Mater*. 2005;21:962–970.
34. Kloosterboer JG. Network formation by chain crosslinking photopolymerization and its applications in electronics. *Adv Polym Sci*. 1988;84:1–61.
35. O'Brien AK, Bowman CN. Impact of oxygen on photopolymerization kinetics and polymer structure. *Macromolecules*. 2006;39: 2501–2506.
36. O'Brien AK, Cramer NB, Bowman CN. Oxygen inhibition in thiol-acrylate photopolymerizations. *J Polym Sci Part A: Polym Chem*. 2006;44:2007–2014.
37. O'Brien AK, Bowman CN. Modeling the effect of oxygen on photopolymerization kinetics. *Macromol Theory Simul*. 2006;15:176–182.
38. Gou LJ, Opheim B, Coretsopoulos CN, Scranton AB. Consumption of the molecular oxygen in polymerization systems using photosensitized oxidation of dimethylanthracene. *Chem Eng Commun*. 2006;193:620–627.
39. Bowman CN, Peppas NA. Coupling of kinetics and volume relaxation during polymerizations of multiacrylates and multimethacrylates. *Macromolecules*. 1991;24:1914–1920.
40. Scranton AB, Bowman CN, Klier J, Peppas NA. Polymerization reaction dynamics of ethylene-glycol methacrylates and dimethacrylates by calorimetry. *Polymer*. 1992;33:1683–1689.
41. Cook WD. Thermal aspects of the kinetics of dimethacrylate photopolymerization. *Polymer*. 1992;33:2152–2161.
42. Tulig TJ, Tirrell M. Toward a molecular theory of the trommsdorff effect. *Macromolecules*. 1981;14:1501–1511.
43. Ballard MJ, Napper DH, Gilbert RG, Sangster DF. Termination-rate coefficients in methyl-methacrylate polymerizations. *J Polym Sci Part A: Polym Chem*. 1986;24:1027–1041.
44. Russell GT, Napper DH, Gilbert RG. Termination in free-radical polymerizing systems at high conversion. *Macromolecules*. 1988; 21:2133–2140.
45. Buback M, Huckestein B, Russell GT. Modeling of termination in intermediate and high conversion free-radical polymerizations. *Macromol Chem Phys*. 1994;195:539–554.
46. Anseth KS, Wang CM, Bowman CN. Reaction behavior and kinetic constants for photopolymerizations of multi(meth)acrylate monomers. *Polymer*. 1994;35:3243–3250.
47. Anseth KS, Wang CM, Bowman CN. Kinetic evidence of reaction-diffusion during the polymerization of multi(meth)acrylate monomers. *Macromolecules*. 1994;27:650–655.
48. Anseth KS, Kline LM, Walker TA, Anderson KJ, Bowman CN. Reaction-kinetics and volume relaxation during polymerizations of multiethylene glycol dimethacrylates. *Macromolecules*. 1995;28: 2491–2499.
49. O'Neil GA, Torkelson JM. Modeling insight into the diffusion-limited cause of the gel effect in free radical polymerization. *Macromolecules*. 1999;32:411–422.
50. Anseth KS, Rothenberg MD, Bowman CN. A photochromic technique to study polymer network volume distributions and microstructure during photopolymerizations. *Macromolecules*. 1994;27: 2890–2892.
51. Goodner MD, Bowman CN. Modeling primary radical termination and its effects on autoacceleration in photopolymerization kinetics. *Macromolecules*. 1999;32:6552–6559.
52. Goodner MD, Bowman CN. Development of a comprehensive free radical photopolymerization model incorporating heat and mass transfer effects in thick films. *Chem Eng Sci*. 2002;57:887–900.
53. Dusek K, Spevacek J. Cyclization in vinyl-divinyl copolymerization. *Polymer*. 1980;21:750–756.
54. Allen PEM, Simon GP, Williams DRG, Williams EH. Dynamic-mechanical properties and cross-polarized, proton-enhanced, magic angle spinning c-13 nmr time constants of poly[oligo(ethylene glycol) dimethacrylates]. *Macromolecules*. 1989;22:809–816.
55. Kannurpatti AR, Anderson KJ, Anseth JW, Bowman CN. Use of "living'' radical polymerizations to study the structural evolution and properties of highly crosslinked polymer networks. *J Polym Sci Part B: Polym Phys*. 1997;35:2297–2307.
56. Kannurpatti AR, Bowman CN. Structural evolution of dimethacrylate networks studied by dielectric spectroscopy. *Macromolecules*. 1998;31:3311–3316.
57. Kannurpatti AR, Anseth JW, Bowman CN. A study of the evolution of mechanical properties and structural heterogeneity of polymer networks formed by photopolymerizations of multifunctional (meth)acrylates. *Polymer*. 1998;39:2507–2513.
58. Fouassaier JP, Rabek JF. *Radiation Curing In Polymer Science and Technology*, Vol 4. New York: Elesvier, 1993.
59. Hoyle CE, Lee TY, Roper T. Thiol-enes: chemistry of the past with promise for the future. *J Polym Sci Part A: Polym Chem*. 2004;42: 5301–5338.

60. Miller GA, Gou L, Narayanan V, Scranton AB. Modeling of photobleaching for the photoinitiation of thick polymerization systems. *J Polym Sci Part A: Polym Chem*. 2002;40:793–808.
61. Kurdikar DL, Peppas NA. Method of determination of initiator efficiency - application to uv polymerizations using 2,2-dimethoxy-2-phenylacetophenone. *Macromolecules*. 1994;27:733–738.
62. Russell GT, Gilbert RG, Napper DH. Chain-length-dependent termination rate-processes in free-radical polymerizations, Part 1: Theory. *Macromolecules*. 1992;25:2459–2469.
63. Buback M, Gilbert RG, Russell GT, Hill DJT, Moad G, Odriscoll KF, Shen J, Winnik MA. Consistent values of rate parameters in free-radical polymerization systems, Part 2: Outstanding dilemmas and recommendations. *J Polym Sci Part A: Polym Chem*. 1992;30: 851–863.
64. Elliott JE, Bowman CN. Monomer functionality and polymer network formation. *Macromolecules*. 2001;34:4642–4649.
65. Elliott JE, Lovell LG, Bowman CN. Primary cyclization in the polymerization of bis-GMA and TEGDMA: a modeling approach to understanding the cure of dental resins. *Dent Mater*. 2001;17:221–229.
66. Elliott JE, Macdonald M, Nie J, Bowman CN. Structure and swelling of poly(acrylic acid) hydrogels: effect of pH, ionic strength, and dilution on the crosslinked polymer structure. *Polymer*. 2004;45:1503–1510.
67. Zhu S, Tian Y, Hamielec AE, Eaton DR. Radical trapping and termination in free-radical polymerization of Mma. *Macromolecules*. 1990;23:1144–1150.
68. Anseth KS, Anderson KJ, Bowman CN. Radical concentrations, environments, and reactivities during crosslinking polymerizations. *Macromol Chem Phys*. 1996;197:833–848.
69. Berchtold KA, Randolph TW, Bowman CN. Propagation and termination kinetics of cross-linking photopolymerizations studied using electron paramagnetic resonance spectroscopy in conjunction with near IR spectroscopy. *Macromolecules*. 2005;38:6954–6964.
70. Zhu S, Hamielec AE. Chain-length-dependent termination for free-radical polymerization. *Macromolecules*. 1989;22:3093–3098.
71. Berchtold KA, Hacioglu B, Lovell L, Nie J, Bowman CN. Using changes in initiation and chain transfer rates to probe the kinetics of cross-linking photopolymerizations: effects of chain length dependent termination. *Macromolecules*. 2001;34:5103–5111.
72. Berchtold KA, Lovell LG, Nie J, Hacioglu B, Bowman CN. The significance of chain length dependent termination in cross-linking polymerizations. *Polymer*. 2001;42:4925–4929.
73. Berchtold KA, Lovestead TM, Bowman CN. Coupling chain length dependent and reaction diffusion controlled termination in the free radical polymerization of multivinyl (meth)acrylates. *Macromolecules*. 2002;35:7968–7975.
74. Lu H, Lovell LG, Bowman CN. Exploiting the heterogeneity of cross-linked photopolymers to create High-T-g polymers from polymerizations performed at ambient conditions. *Macromolecules*. 2001;34:8021–8025.
75. Lovell LG, Lu H, Elliott JE, Stansbury JW, Bowman CN. The effect of cure rate on the mechanical properties of dental resins. *Dent Mater*. 2001;17:504–511.
76. Kloosterboer JG, Vandehei GMM, Boots HMJ. Inhomogeneity during the photopolymerization of diacrylates—Dsc experiments and percolation theory. *Polym Commun*. 1984;25:354–357.
77. Hutchison JB, Lindquist AS, Anseth KS. Experimental characterization of structural features during radical chain homopolymerization of multifunctional monomers prior to macroscopic gelation. *Macromolecules*. 2004;37:3823–3831.
78. Smoluchowski MV. *Versuch einer mathematischen Theorie der Koagulationskinetik kolloider Lösungen*. 1918;92:129–168.
79. Young JS, Bowman CN. Effect of polymerization temperature and cross-linker concentration on reaction diffusion controlled termination. *Macromolecules*. 1999;32:6073–6081.
80. Lovestead TM, Berchtold KA, Bowman CN. Modeling the effects of chain length on the termination kinetics in multivinyl photopolymerizations. *Macromolecul Theory Simul*. 2002;11:729–738.
81. Lovestead TM, Berchtold KA, Bowman CN. An investigation of chain length dependent termination and reaction diffusion controlled termination during the free radical photopolymerization of multivinyl monomers. *Macromolecules*. 2005;38:6374–6381.
82. Lovestead TM, Bowman CN. A modeling investigation of chain length dependent termination during multivinyl free radical chain photopolymerizations: accounting for the gel. *Macromolecules*. 2005;38:4913–4918.
83. Goodner MD, Lee HR, Bowman CN. Method for determining the kinetic parameters in diffusion-controlled free-radical homopolymerizations. *Ind Eng Chem Res*. 1997;36:1247–1252.
84. O'Brien AK, Bowman CN. Modeling thermal and optical effects on photopolymerization systems. *Macromolecules*. 2003;36:7777–7782.
85. Johnson PM, Stansbury JW, Bowman CN. Alkyl chain length effects on copolymerization kinetics of a monoacrylate with hexanediol diacrylate. *J Combin Chem*. 2007;9:1149–1156.
86. Johnson PM, Stansbury JW, Bowman CN. Photopolyrner kinetics using light intensity gradients in high-throughput conversion analysis. *Polymer*. 2007;48:6319–6324.
87. Johnson PM, Stansbury JW, Bowman CN. High-throughput kinetic analysis of acrylate and thiol-ene photopolymerization using temperature and exposure time gradients. *J Polym Sci Part A: Polym Chem*. 2008;46:1502–1509.
88. Johnson PM, Stansbury JW, Bowman CN. Kinetic modeling of a comonomer photopolymerization system using high-throughput conversion data. *Macromolecules*. 2008;41:230–237.
89. Guymon CA, Bowman CN. Kinetic analysis of polymerization rate acceleration during the formation of polymer/smectic liquid crystal composites. *Macromolecules*. 1997;30:5271–5278.
90. Guymon CA, Bowman CN. Polymerization behavior and kinetics during the formation of polymer-stabilized ferroelectric liquid crystals. *Macromolecules*. 1997;30:1594–1600.
91. Guymon CA, Hoggan EN, Clark NA, Rieker TP, Walba DM, Bowman CN. Effects of monomer structure on their organization and polymerization in a smectic liquid crystal. *Science*. 1997;275: 57–59.
92. Cramer NB, Beckel ER, Harant AW, Davies T, Williamson DL, Bowman CN. Formation of a host nanostructure for ferroelectric liquid crystals using thiol-ene polymers. *Liq Cryst*. 2002;29:1291–1296.
93. Beckel ER, Nie J, Stansbury JW, Bowman CN. Effect of aryl substituents on the reactivity of phenyl carbamate acrylate monomers. *Macromolecules*. 2004;37:4062–4069.
94. Beckel ER, Stansbury JW, Bowman CN. Evaluation of a potential ionic contribution to the polymerization of highly reactive (meth)-acrylate monomers. *Macromolecules*. 2005;38:9474–9481.
95. Lu H, Stansbury JW, Nie J, Berchtold KA, Bowman CN. Development of highly reactive mono-(meth)acrylates as reactive diluents for dimethacrylate-based dental resin systems. *Biomaterials*. 2005; 26:1329–1336.
96. Kilambi H, Reddy SK, Schneidewind L, Lee TY, Stansbury JW, Bowman CN. Design, development, and evaluation of monovinyl acrylates characterized by secondary functionalities as reactive diluents to diacrylates. *Macromolecules*. 2007;40:6112–6118.
97. Kilambi H, Reddy SK, Beckel ER, Stansbury JW, Bowman CN. Influence of secondary functionalities on the reaction behavior of monovinyl (meth)acrylates. *Chem Mater*. 2007;19:641–643.
98. Kannurpatti AR, Lu SX, Bunker GM, Bowman CN. Kinetic and mechanistic studies of iniferter photopolymerizations. *Macromolecules*. 1996;29:7310–7315.
99. Cramer NB, Bowman CN. Kinetics of thiol-ene and thiol-acrylate photopolymerizations with real-time Fourier transform infrared. *J Polym Sci Part A: Polym Chem*. 2001;39:3311–3319.
100. Cramer NB, Scott JP, Bowman CN. Photopolymerizations of thiol-ene polymers without photoinitiators. *Macromolecules*. 2002;35: 5361–5365.
101. Cramer NB, Davies T, O'Brien AK, Bowman CN. Mechanism and modeling of a thiol-ene photopolymerization. *Macromolecules.* 2003; 36:4631–4636.
102. Kilambi H, Reddy SK, Schneidewind L, Stansbury JW, Bowman CN. Copolymerization and dark polymerization studies for photopolymerization of novel acrylic monomers. *Polymer*. 2007;48: 2014–2021.
103. Jansen J, Dias AA, Dorschu M, Coussens B. Fast monomers: factors affecting the inherent reactivity of acrylate monomers in photoinitiated acrylate polymerization. *Macromolecules*. 2003;36: 3861–3873.
104. Kilambi H, Stansbury JW, Bowman CN. Deconvoluting the impact of intermolecular and intramolecular interactions on the polymer-

ization kinetics of ultrarapid mono(meth)acrylates. *Macromolecules*. 2007;40:47–54.
105. Kilambi H, Stansbury JW, Bowman CN. Enhanced reactivity of monovinyl acrylates characterized by secondary functionalities toward photopolymerization and Michael addition: contribution of intramolecular effects. *J Polym Sci Part A: Polym Chem*. 2008; 46:3452–3458.
106. Lovell LG, Stansbury JW, Syrpes DC, Bowman CN. Effects of composition and reactivity on the reaction kinetics of dimethacrylate dimethacrylate copolymerizations. *Macromolecules*. 1999;32: 3913–3921.
107. Kilambi H, Cramer NB, Schneidewind LH, Shah P, Stansbury JW, Bowman CN. Evaluation of highly reactive mono-methacrylates as reactive diluents for BisGMA-based dental composites. *Dent Mater*. In press. doi: 10.1016/j.dental.2008.05.003.
108. Morgan CR, Magnotta F, Ketley AD. Thiol-ene photo-curable polymers. *J Polym Sci Part A: Polym Chem*. 1977;15:627–645.
109. Jacobine AF, Glaser DM, Grabek PJ, Mancini D, Masterson M, Nakos ST, Rakas MA, Woods JG. Photocrosslinked norbornene thiol copolymers—Synthesis, mechanical-properties, and cure studies. *J Appl Polym Sci*. 1992;45:471–485.
110. Jacobine AF. *Radiation Curing In Polymer Science and Technology III*. London: Elsevier, 1993.
111. Cramer NB, Reddy SK, O'Brien AK, Bowman CN. Thiol-ene photopolymerization mechanism and rate limiting step changes for various vinyl functional group chemistries. *Macromolecules*. 2003; 36:7964–7969.
112. Reddy SK, Cramer NB, O'Brien AK, Cross T, Raj R, Bowman CN. Rate mechanisms of a novel thiol-ene photopolymerization reaction. *Macromol Symp*. 2004;206:361–374.
113. Cramer NB, Reddy SK, Cole M, Hoyle C, Bowman CN. Initiation and kinetics of thiol-ene photopolymerizations without photoinitiators. *J Polym Sci Part A: Polym Chem*. 2004;42:5817–5826.
114. Reddy SK, Cramer NB, Bowman CN. Thiol-vinyl mechanisms, Part 1: Termination and propagation kinetics in thiol-ene photopolymerizations. *Macromolecules*. 2006;39:3673–3680.
115. Reddy SK, Cramer NB, Bowman CN. Thiol-vinyl mechanisms, Part 2: Kinetic modeling of ternary thiol-vinyl photopolymerizations. *Macromolecules*. 2006;39:3681–3687.
116. Scott TF, Kloxin CJ, Draughon RB, Bowman CN. Nonclassical dependence of polymerization rate on initiation rate observed in thiol-ene photopolymerizations. *Macromolecules*. 2008;41:2987–2989.
117. Reddy SK, Anseth KS, Bowman CN. Modeling of network degradation in mixed step-chain-growth polymerizations. *Polymer*. 2005;46:4212–4222.
118. Okay O, Bowman CN. Kinetic modeling of thiol-ene reactions with both step and chain-growth aspects. *Macromol Theory Simul*. 2005;14:267–277.
119. Okay O, Reddy SK, Bowman CN. Molecular weight development during thiol-ene photopolymerizations. *Macromolecules*. 2005;38: 4501–4511.
120. Reddy SK, Okay O, Bowman CN. Network development in mixed step-chain-growth thiol-vinyl photopolymerizations. *Macromolecules*. 2006;39:8832–8843.
121. Reddy SK, Cramer NB, Cross T, Raj R, Bowman CN. Polymer-derived ceramic materials from thiol-ene photopolymerizations. *Chem Mater*. 2003;15:4257–4261.
122. Cramer NB, Reddy SK, Lu H, Cross T, Raj R, Bowman CN. Thiol-ene photopolymerization of polymer-derived ceramic precursors. *J Polym Sci Part A: Polym Chem*. 2004;42:1752–1757.
123. Carioscia JA, Lu H, Stanbury JW, Bowman CN. Thiol-ene oligomers as dental restorative materials. *Dent Mater*. 2005;21:1137–1143.
124. Carioscia JA, Schneidewind L, O'Brien C, Ely R, Feeser C, Cramer N, Bowman CN. Thiol-norbornene materials: approaches to develop high T-g thiol-ene polymers. *J Polym Sci Part A: Polym Chem*. 2007;45:5686–5696.
125. Rydholm AE, Reddy SK, Anseth KS, Bowman CN. Controlling network structure in degradable thiol-acrylate biomaterials to tune mass loss behavior. *Biomacromolecules*. 2006;7:2827–2836.
126. Rydholm AE, Reddy SK, Anseth KS, Bowman CN. Development and characterization of degradable thiol-allyl ether photopolymers. *Polymer*. 2007;48:4589–4600.
127. Reddy SK, Sebra RP, Anseth KS, Bowman CN. Living radical photopolymerization induced grafting on thiol-ene based substrates. *J Polym Sci Part A: Polym Chem*. 2005;43:2134–2144.
128. Good BT, Reddy S, Davis RH, Bowman CN. Tallorable low modulus, reversibly deformable elastomeric thiol-ene materials for microfluidic applications. *Sensor Actuator B-Chem*. 2007;120:473–480.
129. Khire VS, Benoit DSW, Anseth KS, Bowman CN. Ultrathin gradient films using thiol-ene polymerizations. *J Polym Sci Part A: Polym Chem*. 2006;44:7027–7039.
130. Chiou BS, Kham SA. Real-time FTIR and in situ rheological studies on the UV curing kinetics of thiol-ene polymers. *Macromolecules*. 1997;30:7322–7328.
131. Yi YW, Khire V, Bowman CN, Maclennan JE, Clark NA. Organization of liquid crystals on submicron scale topographic patterns with fourfold symmetry prepared by thiolene photopolymerization-based nanoimprint lithography. *J Appl Phys*. 2008;103:093508–093518.
132. Reddy SK, Cramer NB, Kalvaitas M, Lee TY, Bowman CN. Mechanistic modelling and network properties of ternary thiol-vinyl photopolymerizations. *Aust J Chem*. 2006;59:586–593.
133. Lee TY, Smith Z, Reddy SK, Cramer NB, Bowman CN. Thiol-allyl ether-methacrylate ternary systems. Polymerization mechanism. *Macromolecules*. 2007;40:1466–1472.
134. Lee TY, Carioscia J, Smith Z, Bowman CN. Thiol-allyl ether-methacrylate ternary systems. Evolution mechanism of polymerization-induced shrinkage stress and mechanical properties. *Macromolecules*. 2007;40:1473–1479.
135. Scott TF, Schneider AD, Cook WD, Bowman CN. Photoinduced plasticity in cross-linked polymers. *Science*. 2005;308:1615–1617.
136. Scott TF, Draughon RB, Bowman CN. Actuation in crosslinked polymers via photoinduced stress relaxation. *Adv Mater*. 2006; 18:2128.
137. Anseth KS, Bowman CN. Kinetic gelation model predictions of cross-linked polymer network microstructure. *Chem Eng Sci*. 1994;49:2207–2217.
138. Bowman CN, Peppas NA. Initiation and termination mechanisms in kinetic gelation simulations. *J Polym Sci Part A: Polym Chem*. 1991;29:1575–1583.
139. Bowman CN, Peppas NA. A kinetic gelation method for the simulation of free-radical polymerizations. *Chem Eng Sci*. 1992;47: 1411–1419.
140. Anseth KS, Bowman CN. Kinetic gelation predictions of species aggregation in tetrafunctional monomer polymerizations. *J Polym Sci Part B: Polym Phys*. 1995;33:1769–1780.
141. Flory P. *Principles of Polymer Chemistry*. Ithaca, NY: Corenell University Press, 1953.
142. Stockmayer WH. Theory of molecular size distribution and gel formation in branched-chain polymers. *J Chem Phys*. 1943;11:45–55.
143. Elliott JE, Bowman CN. Kinetics of primary cyclization reactions in cross-linked polymers: an analytical and numerical approach to heterogeneity in network formation. *Macromolecules*. 1999;32: 8621–8628.
144. Elliott JE, Bowman CN. Effect of primary cyclization on free radical polymerization kinetics: modeling approach. *Macromolecules*. 2002;35:7125–7131.
145. Elliott JE, Bowman CN. Predicting network formation of free radical polymerization of multifunctional monomers. *Polym React Eng*. 2002;10:1–19.
146. Elliott JE, Anseth JW, Bowman CN. Kinetic modeling of the effect of solvent concentration on primary cyclization during polymerization of multifunctional monomers. *Chem Eng Sci*. 2001;56: 3173–3184.
147. Young JS, Kannurpatti AR, Bowman CN. Effect of comonomer concentration and functionality on photopolymerization rates, mechanical properties and heterogeneity of the polymer. *Macromol Chem Phys*. 1998;199:1043–1049.
148. Otsu T. Vinyl Polymerization, Part 19: The preparation of block and graft copolymers using some sulfur compounds. *J Polym Sci*. 1957;26:236–239.
149. Otsu T, Ogawa T, Yamamoto T. Solid-phase block copolymer synthesis by the iniferter technique. *Macromolecules*. 1986;19:2087–2089.
150. Kuriyama A, Otsu T. Living radical polymerization of methylmethacrylate with a tetrafunctional photoiniferter—synthesis of a star polymer. *Polym J*. 1984;16:511–514.
151. Otsu T, Yoshida M. Role of initiator-transfer agent-terminator (iniferter) in radical polymerizations—polymer design by organic disulfides as iniferters. *Makromol Chem-Rapid Commun*. 1982;3: 127–132.

152. Otsu T. Iniferter concept and living radical polymerization. *J Polym Sci Part A: Polym Chem*. 2000;38:2121–2136.
153. Lovell LG, Elliott BJ, Brown JR, Bowman CN. The effect of wavelength on the polymerization of multi(meth)acrylates with disulfide/benzilketal combinations. *Polymer*. 2001;42:421–429.
154. Sebra RP, Kasko AM, Anseth KS, Bowman CN. Synthesis and photografting of highly pH-responsive polymer chains. *Sensor Actuator B-Chem*. 2006;119:127–134.
155. Sebra RP, Anseth KS, Bowman CN. Integrated surface modification of fully polymeric microfluidic devices using living radical photopolymerization chemistry. *J Polym Sci Part A: Polym Chem*. 2006;44:1404–1413.
156. Lovell LG, Newman SM, Bowman CN. The effects of light intensity, temperature, and comonomer composition on the polymerization behavior of dimethacrylate dental resins. *J Dent Res*. 1999; 78:1469–1476.
157. Lovell LG, Newman SM, Donaldson MM, Bowman CN. The effect of light intensity on double bond conversion and flexural strength of a model, unfilled dental resin. *Dent Mater*. 2003;19: 458–465.
158. Williams G, Watts DC. Non-symmetrical dielectric relaxation behaviour arising from a simple empirical decay function. *Trans Faraday Soc*. 1970;66:80–85.
159. Hall DN, Oswald AA, Griesbau. K. Allene chemistry, Part 4: Unsymmetrical terminal thiol-allene diadducts. Effect of allylic reversal. *J Org Chem*. 1965;30:3829–3834.
160. Hall DN. Role of allylic reversal in free-radical thiol additions to allylic halides. *J Org Chem*. 1967;32:2082–2087.
161. Migita T, Kosugi M, Takayama K, Nakagawa Y. S'h type reactions of substituted allylic compounds. *Tetrahedron*. 1973;29:51–55.
162. Barton DHR, Crich D. The invention of new radical chain-reactions, Part 12: Improved methods for the addition of carbon radicals to substituted allylic groups. *J Chem Soc-Perkin Trans 1*. 1986:1613–1619.
163. Meijs GF, Rizzardo E, Thang SH. Preparation of controlled molecular-weight, olefin-terminated polymers by free-radical methods—chain transfer using allylic sulfides. *Macromolecules*. 1988;21: 3122–3124.
164. Evans RA, Moad G, Rizzardo E, Thang SH. New free-radical ring-opening acrylate monomers. *Macromolecules*. 1994;27:7935–7937.
165. Evans RA, Rizzardo E. Free-radical ring-opening polymerization of cyclic allylic sulfides. *Macromolecules*. 1996;29:6983–6989.
166. Kalipcilar B, Karaagaclioglu L, Hasanreisoglu U. Evaluation of the level of residual monomer in acrylic denture base materials having different polymerization properties. *J Oral Rehabil*. 1991;18:399–401.
167. Vaidyanathan J, Vaidyanathan TK. Interactive effects of resin composition and ambient-temperature of light curing on the percentage conversion, molar heat of cure and hardness of dental composite resins. *J Mater Sci-Mater Med*. 1992;3:19–27.
168. Barron DJ, Rueggeberg FA, Schuster GS. A comparison of monomer conversion and inorganic filler content in visible light-cured denture resins. *Dent Mater*. 1992;8:274–277.
169. Patel MP, Braden M, Davy KWM. Polymerization shrinkage of methacrylate esters. *Biomaterials*. 1987;8:53–56.
170. Bailey WJ. Cationic polymerization with expansion in volume. *J Macromol Sci-Chem A*. 1975;9:849–865.
171. Stansbury JW. Synthesis and evaluation of new oxaspiro monomers for double ring-opening polymerization. *J Dent Res*. 1992;71:1408–1412.
172. Tilbrook DA, Clarke RL, Howle NE, Braden M. Photocurable epoxy-polyol matrices for use in dental composites I. *Biomaterials*. 2000;21:1743–1753.
173. Ge JH, Trujillo-Lemon M, Stansbury JW. A mechanistic and kinetic study of the photoinitiated cationic double ring-opening polymerization of methylene-7-phenyl-1,4,6,9-tetraoxa-spiro[4.4]nonane. *Macromolecules*. 2006;39:8968–8976.
174. Moszner N, Salz U. Recent developments of new components for dental adhesives and composites. *Macromol Mater Eng*. 2007; 292:245–271.
175. Peppas NA, Langer R. New challenges in biomaterials. *Science*. 1994;263:1715–1720.
176. Langer RS, Peppas NA. Present and future applications of biomaterials in controlled drug delivery systems. *Biomaterials*. 1981;2: 201–214.
177. Langer R. New methods of drug delivery. *Science*. 1990;249: 1527–1533.
178. Hubbell JA. Biomaterials in tissue engineering. *Biotechnology*. 1995;13:565–576.
179. Uhrich KE, Cannizzaro SM, Langer RS, Shakesheff KM. Polymeric systems for controlled drug release. *Chem Rev*. 1999;99: 3181–3198.
180. Metters AT, Bowman CN, Anseth KS. A statistical kinetic model for the bulk degradation of PLA-b-PEG-b-PLA hydrogel networks. *J Phys Chem B*. 2000;104:7043–7049.
181. Metters AT, Anseth KS, Bowman CN. Fundamental studies of a novel, biodegradable PEG-b-PLA hydrogel. *Polymer*. 2000;41: 3993–4004.
182. Mason MN, Metters AT, Bowman CN, Anseth KS. Predicting controlled-release behavior of degradable PLA-b-PEG-b-PLA hydrogels. *Macromolecules*. 2001;34:4630–4635.
183. Metters AT, Anseth KS, Bowman CN. A statistical kinetic model for the bulk degradation of PLA-b-PEG-b-PLA hydrogel networks: incorporating network non-idealities. *J Phys Chem B*. 2001;105: 8069–8076.
184. Sebra RP, Masters KS, Bowman CN, Anseth KS. Surface grafted antibodies: controlled architecture permits enhanced antigen detection. *Langmuir*. 2005;21:10907–10911.
185. Sebra RP, Masters KS, Cheung CY, Bowman CN, Anseth KS. Detection of antigens in biologically complex fluids with photografted whole antibodies. *Anal Chem*. 2006;78:3144–3151.
186. Sebra RP, Reddy SK, Masters KS, Bowman CN, Anseth KS. Controlled polymerization chemistry to graft architectures that influence cell-material interactions. *Acta Biomaterialia*. 2007;3:151–161.
187. Hansen RR, Sikes HB, Bowman CN. Visual detection of labeled oligonucleotides using visible-light-polymerization-based amplification. *Biomacromolecules*. 2008;9:355–362.
188. Sikes HD, Hansen RR, Johnson LM, Jenison R, Birks JW, Rowlen KL, Bowman CN. Using polymeric materials to generate an amplified response to molecular recognition events. *Nature Mater*. 2008;7:52–56.
189. Hansen RR, Avens HJ, Shenoy R, Bowman CN. Quantitative evaluation of oligonucleotide surface concentrations using polymer-based amplification. *Anal Bioanal Chem*. 2008;392:167–175.

Manuscript received Aug. 11, 2008.